Optimizing solar energy forecasting in Senegal: sensitivity analysis of WRF-solar radiation schemes

Aissatou Ndiaye, Windmanagda Sawadogo, Jan Bliefernicht, Cheikh Dione, Mounkaila Saley Moussa, Laouali Dungall, Amadou Thierno Gaye, Harald Kunstmann

Angaben zur Veröffentlichung / Publication details:

Ndiaye, Aissatou, Windmanagda Sawadogo, Jan Bliefernicht, Cheikh Dione, Mounkaila Saley Moussa, Laouali Dungall, Amadou Thierno Gaye, and Harald Kunstmann. 2026. "Optimizing solar energy forecasting in Senegal: sensitivity analysis of WRF-solar radiation schemes." *Theoretical and Applied Climatology* 157 (5): 323. https://doi.org/10.1007/s00704-026-06272-1.

Theoretical and Applied Climatology (2026) 157:323
https://doi.org/10.1007/s00704-026-06272-1

RESEARCH

Optimizing solar energy forecasting in Senegal: Sensitivity analysis of WRF-solar radiation schemes

Aissatou Ndiaye[1,4] · Windmanagda Sawadogo[2] · Jan Bliefernicht[1] · Cheikh Dione[3] · Mounkaila Saley Moussa[4,5] · Laouali Dungall[5] · Amadou Thierno Gaye[6] · Harald Kunstmann[1,2,7]

Received: 23 June 2025 / Accepted: 16 April 2026 / Published online: 25 April 2026

Abstract

Solar irradiance forecasting is essential in maximizing solar energy utilization and facilitating the shift towards an eco-friendly and sustainable energy future. However, accurate solar irradiance from numerical weather prediction remains challenging. This research evaluates the performance of state-of-the-art Weather Research and Forecasting tailored to the solar energy applications (WRF-Solar) at two operational solar plants in Senegal: Diass and Ten Merina. The experiments include different shortwave radiation schemes (Dudhia and RRTMG) with RRTMG coupled with dynamic aerosols. In addition, the impact of shallow convection on the different experiments is investigated. A total of six simulations is performed and assessed under various sky conditions using hourly GHI measurements for 2020. Results indicate that the RRTMG scheme coupled with aerosols outperforms other simulations, exhibiting a maximum correlation (R) of 0.85, skill score (SS) of 0.17, and the lowest RMSE value (160 W/m^2) and MAE (110 W/m^2). However, WRF-Solar exhibits poor performance across all experiments (RMSE = 386 W/m², R = 0.55, SS = -1.48) under cloudy skies. The influence of the shallow convection scheme in the WRF-Solar model on GHI estimation was found to be limited under different atmospheric conditions at both sites. These findings offer valuable insights that can enhance solar energy forecasting accuracy and support reliable solar power generation and renewable energy optimization, benefiting energy providers, policymakers, and communities in Senegal.

1 Introduction

With respect to the Paris Agreement and the cost reduction of renewable technologies, many countries are increasing their renewable energy capacity as part of climate change mitigation efforts. 183 Parties incorporated renewable energy components in their Nationally Determined Contributions (NDCs) in 2022, with 108 of them having set targets for renewable energy in the power sector (IRENA 2022). Senegal's strategic plan aims to inject an additional 699 MW of renewable energy into the grid by 2030 (UNFCCC 2020).

The effectiveness of renewable energy supplies in reducing CO2 emissions is due to their minimal carbon footprint, with carbon emissions per unit of generated energy typically between 1 and 10% of those of fossil fuels (Moomaw et al. 2011). Renewable energy deployments have grown in recent years (2010–2020). The African continent is seeing a 7% increase in renewale energy-based generation capacity, of which solar energy had the largest additions (IRENA and AfDB, 2022). About 10 solar PV plants have been implemented in Senegal since 2016. However, like other

✉ Aissatou Ndiaye
aissatou.ndiaye@uni-a.de

1 Chair for Regional Climate and Hydrology, Institute of Geography, University of Augsburg, 86135 Augsburg, Germany

2 Institute of Meteorology and Climate Research, Karlsruhe Institute of Technology, Campus Alpin, 82467 Garmisch-Partenkirchen, Germany

3 Institut Pierre Simon Laplace (IPSL), Université de Sorbonne, Paris, France

4 West African Science Service Center on Climate Change and Adapted Land Uses (WASCAL), Abdou Moumouni University, BP 10662, Niamey, Niger

5 Department of Physics, Faculty of Sciences and Techniques, Abdou Moumouni University, BP 10662, Niamey, Niger

6 Laboratoire de Physique de l'Atmosphère et de l'Océan Siméon Fongang, BP 5085, Dakar-Fann, Dakar, Sénégal

7 Center for Climate Resilience, University of Augsburg, 86135 Augsburg, Germany

renewable energy sources, solar energy is influenced by weather and climate conditions. To estimate or forecast the production of a solar PV plant, climate information, such as solar irradiance, is necessary.

In Africa, meteorological data and analytical resources have been constrained by a shortage of relevant expertise to generate useful information or difficulties in obtaining existing data (Dinku 2019; Bliefernicht et al. 2018). Although the National Meteorological and Hydrological Services (NMHSs) are mandated to provide and share national data, in Africa, data sharing with other institutions is quite limited and usually involves the cost of provision if available (Dinku 2019; Overpeck et al. 2011). In Senegal, the renewable energy sector lacks access to climate information and usually relies on online platforms for their data needs. This climate information, however, is vital for effective management and planning of renewable energy resources.

Solar energy forecasting is essential for utilities that rely on solar power generation to provide customers with a reliable and cost-efficient electricity supply. Due to its intermittent nature, integrating solar energy into the grid remains challenging. Accurate solar PV forecasting supports grid stability by enabling operators to accurately predict the amount of energy that PV systems will generate over a given period (Benitez et al. 2023). Numerical Weather Prediction (NWP) could be an alternative. It is an essential tool for forecasting solar irradiance beyond a few hours, aiding in scheduling solar power plants for the day ahead (Larson 2013). NWP models use atmospheric reanalysis to establish the initial and lateral boundary conditions and generate forecasts of meteorological variables, including temperature, relative humidity, and wind speed. Incorporating weather parameters has been shown to improve the accuracy of solar irradiance estimation, and consequently solar PV output forecasting (Gavina et al. 2024).

The Weather Research and Forecasting model for solar energy applications (WRF-solar) is a NWP that has been used in many studies for GHI forecasts (e.g., Lara-Fanego et al. 2012; Lee et al. 2017; Verbois et al. 2018; Gueymard and Jimenez 2019; Prasad and Kay 2020; Sawadogo et al. 2023; Sawadogo et al. 2024). WRF-Solar is the first NWP model specifically tailored for solar energy purposes (Jimenez et al. 2016). It is an improved version of the WRF model. It caters to the growing need for tailored NWP products in the solar energy sector (Jimenez et al. 2016). The WRF model has been improved and adjusted to better model the interaction of aerosols, clouds, and radiation, which helps decrease the prediction uncertainty of GHI (Haupt et al.2016). Numerous studies on the WRF-Solar model have been conducted worldwide. Arbizu-Barrena et al. (2017) employed a new technique called Cloud Index Advection and Diffusion in Spain to forecast short-term solar radiation, integrating the precision of satellite-based cloud representation with the WRF model's ability to simulate atmospheric dynamics. In Australia, Mukkavilli et al. (2018) compared various physical parameterization schemes to predict hourly direct normal irradiance under different aerosol conditions. Studies for the USA, Gamarro et al. (2019) and Lee et al. (2017) integrated the WRF-Solar modifications with a multilayer energy model to develop a harmonized WRF forecasting systems known as urban WRF-Solar and evaluated WRF-solar alongside four different nowcasting models for GHI forecast in California, respectively. Compared to WRF, which has been frequently used by several authors (Abdallah et al. 2015; Nooni et al. 2022; Diaz et al. 2015; Arnault et al. 2016; Klein et al. 2015; D'Isidoro et al. 2020; Zhao et al. 2011), the use of WRF Solar is very limited in Africa. Some studies for Senegal using WRF looked at dust concentration ($PM_{2.5}$, PM_{10}) to assess air quality and its impacts on respiratory well-being (Toure et al. 2019; Diokhane et al. 2016; Jenkins et al. 2022). In another study, the MM5 and WRF mesoscale models were used to replicate intense precipitation and low-temperature events in Senegal, focusing on intense off-season rains (Fall et al. 2007). Recently, one of the first WRF-Solar applications was done by Sawadogo et al. (2023), who evaluated various shortwave radiation schemes within the WRF-Solar model for simulating GHI in West Africa, specifically in Ghana and the southern region of Burkina Faso.

Despite these advances, little is known about WRF-Solar performance in Senegal's Sahelian climate, which is characterized by high aerosol from frequent dust events (Toure et al. 2019). A detailed evaluation of different radiation schemes and model configurations is needed to improve solar irradiance forecasting in this unique environment. The studies of Sawadogo et al. (2023) focused on different climate zones (Guinea and Savannah). Senegal is located in the Sahel region; evaluating the model in this climate zone will provide a more comprehensive understanding and offer a clearer overview of the WRF-Solar model's performance in West Africa. This gap is particularly critical as reliable solar forecasts are essential for integrating solar power into electricity grids and reducing stability challenges. In Senegal, improving the accuracy of solar irradiance forecasts can support the expansion of renewable energy, making the evaluation of WRF-Solar performance in this country important.

This study advances solar irradiance forecasting for data scarce regions of West Africa in several important ways. First, it provides the first evaluation of WRF-Solar at operational solar power plants in Senegal, a country strongly influenced by mineral dust and seasonal biomass burning aerosols. Second, it presents the first assessment of the role of shallow convection parameterizations on WRF-Solar

performance in tropical West Africa. Third, the study demonstrates that dynamically incorporating aerosol optical depth substantially improves solar irradiance forecast accuracy under real world operational conditions, showing the importance of aerosol-radiation interactions in regions with high aerosols.

Therefore, this study aims to assess WRF-Solar performance for solar irradiance estimation in Senegal. This is done by performing multiple WRF-Solar simulations (six) using different shortwave radiation schemes (Dudhia and RRTMG) and aerosol information. For the RRTMG scheme, two simulations are carried out: one without aerosol optical depth (AOD) and one with AOD (RRTMG_AERO). Moreover, we examine the impacts of shallow convection on the different simulations. In fact, Deng's shallow scheme can generate reasonable cloud fractions and decrease surface temperature bias, which can have an impact on surface radiation (Deng et al. 2014). Different experiments with or without the activation of shallow convection are assessed under two operational solar plants: Diass and Ten Merina. To evaluate the performance of WRF-Solar, all the analyses are assessed under different atmospheric conditions (clear-sky, cloudy-sky, all-sky, and high aerosol concentration). The results of the study contribute to the knowledge of the performance of the WRF-Solar model in areas located in the Sahel region that are prone to high aerosol episodes.

2 Materials and methods

2.1 Study area and observation data

The research focuses on two solar plants in Senegal. Senegal is located between latitudes 12° − 17° N and longitudes 11° − 18° W (Fig. 1). The country spans an area of approximately 196,700 km^2 and has a coastline of about 700 km. The climate is tropical, regulated by the Intertropical Convergence Zone (ITCZ), with a long dry season from October to May (Sarr et al. 2014). During the rainy season (June-September), the ITCZ moves northwards, and the southern region receives more rainfall than the northern region. The country has high solar energy resources, receiving about 3000 h of sunshine yearly, with an average solar energy estimate of approximately 2000 kWh/m^2/year (Youm et al. 2000). Dust events in Senegal are common due to the country's proximity to the Sahara Desert. These events typically occur during the dry season, when strong Harmattan winds carry dust across the region (Jenkins et al. 2022).

Ground-based GHI data were used to evaluate the model (Table 1). The ground-based hourly GHI data were collected from two solar plants (Diass and Ten Merina), all located in the region of Thies. Thies is about 50 km from the capital city of Dakar and is characterized by an annual rainfall between 500 and 650 mm, a semi-arid climate, and a mean annual temperature of 26.7° C (Senghor et al. 2011). The solar plants are on-grid with an installed capacity of 23 MW and 30 MW, respectively. They are equipped with meteorological stations, including pyranometers, which take measurements of the GHI. Since access to data remains a major challenge in Africa, the selection of these plants was primarily driven by data availability. Additionally, Ten Merina is located inland, whereas Diass is closer to the coast, a contrast that may also play an important role in the analysis.

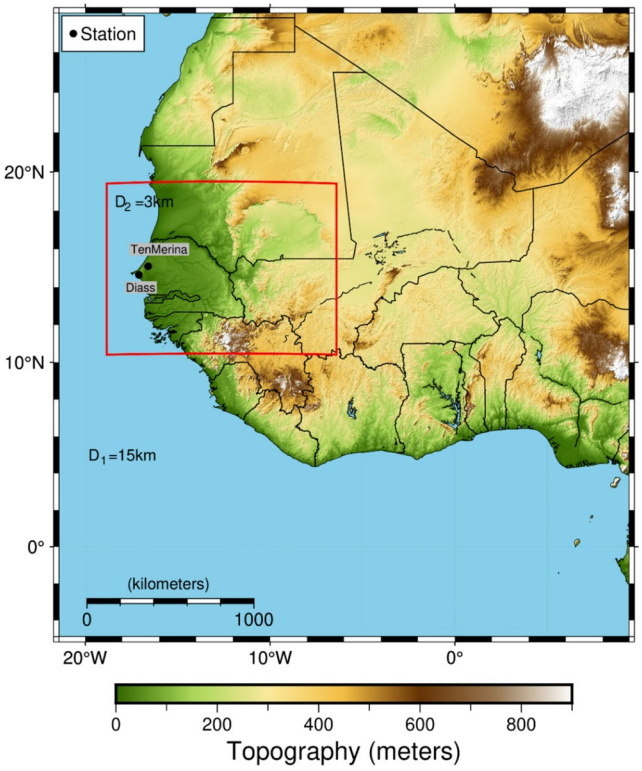

Fig. 1 WRF domains showing the two domains: the domain (D1) with 15 km of resolution and the domain (D2) with 3 km of resolution

Table 1 is a summary of all the dataset used in this study

	Reference	Resolution	Period
ERA5	Hersbach et al. 2020	31 Km/hourly	2020
CAMS	Peuch et al. 2022	40 Km/3hourly	
Observation	Solar Plants	Point Coordinate/hourly	

2.2 Model data

2.2.1 Era5 data

ERA5 reanalysis data were used to define the model's boundary conditions. It is a reanalysis dataset produced by

the European Centre for Medium-Range Weather Forecasts (ECMWF) as part of the Copernicus Climate Change Service (Hersbach et al. 2020). The ERA5 dataset is the fifth generation ECMWF reanalysis, offering horizontally and vertically improved resolution. Estimates of atmospheric variables are provided by the ERA5 dataset with a global resolution of about 31 km (corresponding to ~0.25° grid spacing). The reanalysis datasets used in this study are hourly surface and atmospheric pressure data from 01 st December 2019 to 31 st December 2020.

2.2.2 Copernicus atmosphere monitoring service datasets (CAMS)

The aerosol optical depth (AOD 550 nm) utilized in this study was obtained from CAMS. CAMS utilizes ECMWF's computational systems and forecasting framework to generate global analyses and forecasts of atmospheric composition that are nearly real-time (Peuch et al. 2022). The analyses of the global atmospheric composition of CAMS are based on the ECMWF integrated prediction system and exploit more than 90 different satellite data streams (Peuch et al. 2022). The CAMS system operates at ~40 km horizontal resolution (spectral) and 137 vertical levels (0.01–1013 hPa) (Garrigues et al. 2022). The Ångstrom exponent (α) used in this study is estimated from the linear regression of Eq. 1 (Reid et al. 1999; Knobelspiesse et al. 2004; Schuster et al. 2006) at a different wavelength of 469 and 865 nm. As CAMS does not provide the Ångström exponent at 550 nm, we computed it using Eq. 1 to obtain AOD at this wavelength, which is required for WRF-Solar. The AOD at 469, 550, and 865 nm data are 3-hourly data and cover the period of 01 st December 2019 to 31 st December 2020.

$$\alpha = -\frac{\ln\frac{\tau_{\lambda_1}}{\tau_{\lambda_2}}}{\ln\frac{\lambda_1}{\lambda_2}} \quad (1)$$

τ_{λ_1} and τ_{λ_2} are the total AOD with wavelengths of λ_1 and λ_2, respectively.

2.3 WRF solar model

2.3.1 WRF solar configuration and setup

The WRF-Solar version 4.2.2 was used to assess the model's performance in estimating solar irradiance in Senegal. In this study, we employed a one-way, two-layer nested domain setup: an outer domain (D1 = 15 km), which covers the whole of West Africa, and an inner domain (D2 = 3 km) set over Senegal (Fig. 1). The simulation was done for 2020 at 15 km spatial resolution (coarse resolution) and 3 km (high-resolution), respectively, for D1 and D2. Similar domains have previously been used in West Africa (Fall et al. 2007; Diokhane et al. 2016; Jenkins et al. 2022; Sawadogo et al. 2023). The two domains have grid points of 200 × 220 and 401 × 301, respectively. We incorporated the land use fraction and land use index from MODIS and the green vegetation index from the Fraction of Photosynthetically Active Radiation (FPAR) into the WRF Preprocessing System (WPS). The model's land use was also initialized using GEODATA TOPO (10 M) data from the United States Geological Survey topography database.

2.3.2 WRF experiment

Multiple numerical experiments were performed to evaluate the performance of various parametrizations integrated into WRF-Solar for forecasting solar irradiance. Because WRF-Solar is a physically based NWP model, our analysis directly reflects the atmospheric processes influencing solar irradiance in Senegal. Many factors are considered for the model's physical parameters, including cloud cover, aerosol optical depth, and solar radiation. For a given region, choosing the most appropriate set of physical parameterization options in the model is crucial for any simulation (Patil and Kumar 2016). The appropriate selection ensures a more physically realistic representation in the simulation. The WRF Solar model provides several options for the microphysics scheme. This scheme is used to describe the processes of cloud formation, precipitation, and other microphysical processes in the atmosphere. In this study, we used the state-of-the-art recommendation physics schemes in the WRF-Solar model tailored for solar energy applications. The Thompson microphysics scheme was applied in this study, as it is a reasonable choice for cloud properties simulations (Otkin and Greenwald 2008; Jimenez et al. 2016; Yang et al. 2021). Cumulus schemes account for convective rainfall, while microphysics handles non-convective ones (Aryaputera, 2015). The Cumulus scheme is used to represent the effects of deep convection that occur on a scale too small to be resolved by the model. However, the cumulus scheme has been found to mispresent the sub-grid scale clouds. To improve cloud simulation accuracy, WRF-Solar incorporates a shallow convection scheme. Deng's shallow cumulus parametrization scheme was used to account for the effect of unresolved clouds. Deng's shallow convection scheme employs a mass-flux formulation with explicit cloud entrainment/detrainment dynamics to represent updraft processes. Scheme activation depends on boundary layer depth and turbulent kinetic energy thresholds (Jimenez et al. 2016).

Additional physics parameterizations selected for this study include the Fast All-sky Radiation Model for Solar applications (FARMS), the Mellor-Yamada-Nakanishi-Niino

(MYNN) planetary boundary layer (PBL) scheme, and the Noah Land Surface Model (Niu et al. 2011).

The integration of FARMS facilitates high-temporal-resolution computation of surface solar radiation, significantly improving the model's ability to capture irradiance variability at each time step (Gueymard and Jimenez 2019). It is designed to be computationally efficient while still providing accurate results, making it suitable for weather and climate simulations. The WRF model offers many options for the PBL and Land Surface Model (LSM) schemes. The MYNN scheme represents boundary layer clouds by parameterizing their properties, including the cloud mixing ratio and fraction (Yang et al. 2021). The LSM simulates the exchange of heat, moisture, and momentum across the land-atmosphere interface (Chen and Dudhia 2001).

In this study, six experiments were run to investigate the impacts of two different shortwave radiation schemes (Dudhia and RRTMG) in the model for two solar plants in Senegal (Diass and Ten Merina). Senegal experiences dust episodes originating from the Sahara Desert as well as other aerosol types throughout the year, making it essential to incorporate these factors into the WRF-Solar model. In fact, GHI reaching photovoltaic systems can be significantly reduced by the presence of aerosols (Jimenez et al. 2016). To achieve that, we coupled the WRF-Solar model with time-varying aerosols through the RRTMG shortwave radiation scheme: one without aerosol optical depth (AOD) and one with AOD (RRTMG_AERO). For the RRTMG_AERO simulation, the Thompson and Eidhammer (2014) scheme was applied to enable direct cloud–aerosol feedback. Besides this, we also investigated the impacts of shallow convection on GHI estimation in Senegal. All the experiments were done under no shallow and shallow schemes. Hourly values of GHI were generated from the simulation timeframe spanning from 01 st December 2019 to 31 st December 2020, with December 2019 dedicated to the spin-up process. To ensure reproducibility, all WRF-Solar configurations and simulation parameters are documented in Table 2, and the specific model version (4.2.2) and its source code are provided here https://github.com/wrf-model/WRF/archive/refs/tags/v4.2.2.zip.

Table 2 Parameterization schemes applied in the model configurations

Physics		Dudhia	RRTMG	RRTMG_AERO
Radiation	Shortwave	Dudhia	RRTMG	RRTMG + aerosols
	Longwave	RRTMG	RRTMG	RRTMG
Land surface		Noah land surface model		
Microphysics		Thompson		Thompson and Eidhammer (2014)
PBL		Mellor–Yamada–Nakanishi–Niino (MYNN)		
Shallow cumulus		Deng cumulus		
FARMS		Activated		

2.4 Methods

2.4.1 Quality control of the observation data

The data quality control involves visualizing the hourly GHI throughout the year and removing any missing data and suspicious GHI values. Initially, the raw data consisted of sub-hourly measurements, and the GHI values for each hour were extracted. If any missing values occurred between 20:00 and 5:00 (nighttime) in the raw data, a value of 0 was assigned to them. Nevertheless, if there are any missing values outside this time window, we considered the GHI values for the next three timesteps (t + 1 to t + 3).

Figure 2 illustrates the time series of instantaneous hourly GHI for Diass and Ten Merina stations. These two stations exhibit a similar hourly GHI pattern over the year. The availability of solar resources is highest in the dry period, while the GHI values slightly decrease in the rainy season and some days during Harmattan. However, some missing data points in Diass (4) and Ten Merina (54) were excluded from the analysis. Finally, to identify and exclude recorded data that may be suspicious due to sensor calibration issues or faults, the BSRN (Baseline Surface Radiation Network) tests were applied. The tests identify abnormal GHI measurements that deviate from normal levels. The BSRN guidelines (BSRN 2021) provide the physically feasible range (Eq. 2) and the highly unusual limit (Eq. 3) for GHI measurements:

$$-4\,W/m^2 < GHI < I_0 * 1.5 * cos\,(SZA)^{1.2} + 100\,W/m^2 \quad (2)$$

$$-2\,W/m^2 < GHI < I_0 * 1.5 * cos\,(SZA)^{1.2} + 50\,W/m^2 \quad (3)$$

where I_0 is the solar constant and SZA the solar zenith angle.

2.4.2 Model evaluation

The evaluation of the model involves comparing its outputs with observations to assess its accuracy and reliability in predicting hourly GHI values. A nearest-neighbour interpolation technique was used to identify and extract the simulation data points that match the station's geographical coordinates. When evaluating the performance of various simulations against observational data, the focus was solely on GHI values derived from observations when the solar zenith angle (SZA) is below 85°. This selection criterion was implemented to prevent potential GHI errors caused by measurement uncertainties during dawn and late evening periods, along with the seasonal effects of sunrise and sunset (Sawadogo et al. 2023). For the study

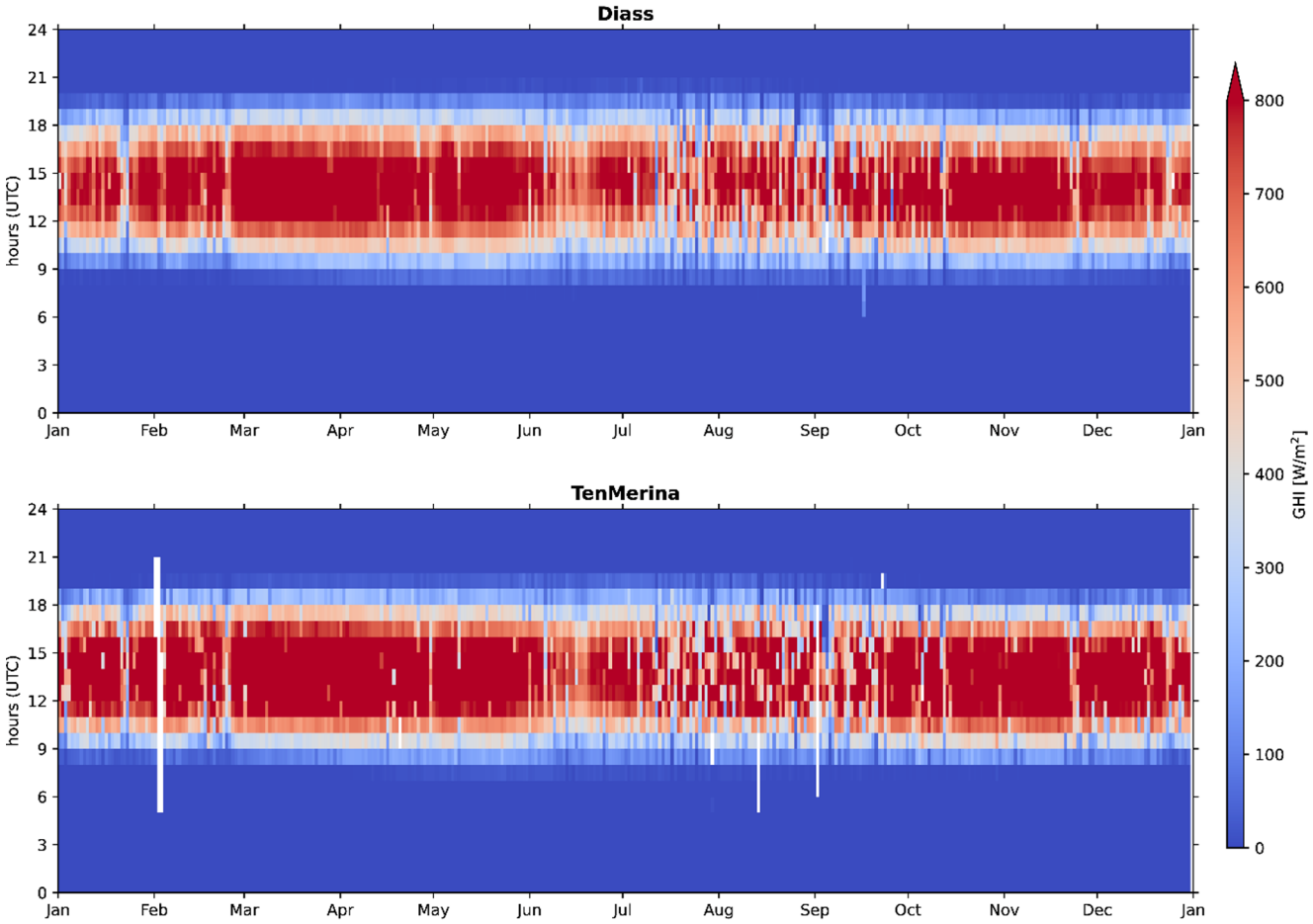

Fig. 2 Time series of instantaneous hourly GHI showing the data variations and availability for the two solar plants before quality control. The white bands represent missing data

region, SZA values < 85° correspond to a Universal Time Coordinated period between 8:00 and 18:00. Our analysis comprised three scenarios: cloudy sky, clear-sky, and all-sky conditions. For both cloudy and clear-sky analyses, the observational data were categorized using the clearness index (Kt) to distinguish composite days with cloudy and clear-sky conditions.

$$Kt = \frac{GHI}{G_0} \tag{4}$$

With GHI being surface-level global horizontal irradiance and G_0 the top-of-atmosphere irradiance.

The clearness index quantifies the proportion of direct solar radiation reaching the Earth. Therefore, the threshold values used to distinguish between cloudy and clear skies may differ based on location. The definition of clear and cloudy sky in this study is based on Kt values, with $Kt \geq 0.65$ indicating clear skies and $Kt \leq 0.4$ indicating cloudy skies.

2.4.3 Evaluation metrics

To evaluate the accuracy of WRF-Solar, we employed multiple statistical metrics: root mean square error (RMSE) and mean absolute error (MAE) to quantify absolute deviations, correlation coefficient (r) to assess linear relationships, and the index of agreement (IOA) to evaluate error magnitudes and temporal alignment. In addition to this, we also calculated the RMSE-based skill score (SS) following Murphy (1988).

For normalized comparisons, we derived nRMSE and nMAE by scaling RMSE and MAE against observed means. The IOA, which ranges from 0 (no agreement) to 1 (perfect match), further validated model skill in replicating both the magnitude and timing of observed irradiance.

$$MAE = \frac{1}{n}\sum_{i=1}^{n}(|p_i - o_i|) \tag{6}$$

$$nMAE = \left[\frac{MAE}{o_{max} - o_{min}}\right] 100 \tag{7}$$

$$RMSE = \sqrt{\sum_{i=1}^{n} \frac{(p_i - o_i)^2}{n}} \tag{8}$$

$$nRMSE = \left[\frac{RMSE}{o_{max} - o_{min}}\right] 100 \tag{9}$$

$$r = \frac{\sum_{i=1}^{n}(o_i - \bar{o})(p_i - \bar{p})}{\sqrt{\sum_{i=1}^{n}(o_i - \bar{o})^2 \sum_{i=1}^{n}(p_i - \bar{p})^2}} \tag{10}$$

$$IOA = 1 - \frac{\sum_{i=1}^{n}(p_i - o_i)}{\sum_{i=1}^{n}\left(\left|p_i - \bar{o}\right| \left|o_i - \bar{o}\right|\right)^2} \tag{11}$$

$$SS = 1 - \frac{RMSE_{(p,0)}}{RMSE_{(r,0)}} \tag{12}$$

where p_i is the simulated GHI, o_i represents the observed GHI at timestep i. The analysis used n data points, with o_{max} and o_{min} indicating the observed maximum and minimum values. $\bar{o}$ and $\bar{p}$ are the average values of the observation and simulation, respectively. r represents the and the reference simulation.

3 Results

3.1 Evaluation of the WRF-solar simulations

3.1.1 Scatter plot of simulated against observed GHI

Figure 3 presents the scatter plot analysis for GHI, which compares the performance of different WRF shortwave radiation schemes, including shallow and no shallow schemes, for the study locations and the entire dataset. In general, the estimated GHI shows minimal or no differences between simulations run with or without the shallow convection scheme under all-sky conditions. For instance, the Dudhia_shallow experiment shows a RMSE of 198 W/m^2 (15%), a MAE of 146 W/m^2 (11%), while the Dudhia_no_shallow indicates 199 W/m^2 (15%) and 146 W/m^2 (11%), respectively, with no difference in the SS (−0.4). Different from the study of Jiménez et al. (2022), who demonstrated that integrating Deng's shallow cumulus parametrization can enhance solar irradiance forecasting even at high resolution in the Contiguous United States (CONUS) domain, our results indicate that the inclusion or exclusion of the shallow convection scheme in the model has minimal influence on GHI estimation at 3 km within the region under all-sky conditions. It is important to note that these discrepancies could be related to the fact that Jiménez et al. (2022) used sub-hourly data, which may capture finer temporal variations of the clouds that are not as evident with instantaneous hourly data.

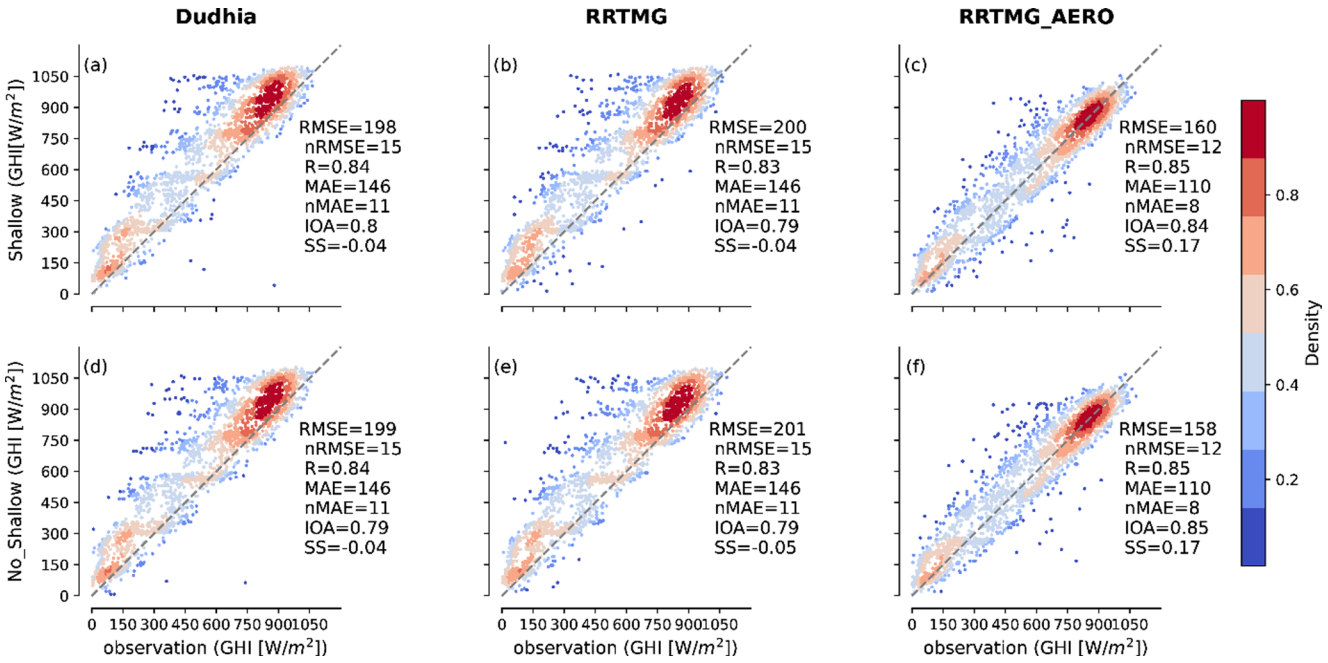

Fig. 3 Scatter plot comparing hourly GHI values from various WRF Solar simulations against observations for the two solar plants

Another reason could be the response of the climate system to the activation of the shallow convection scheme in Senegal, especially in the tropics, where deep convection dominates cloud formation (Danso et al. 2020). This suggests that, under specific atmospheric and regional characteristics, the role of shallow convection in modulating GHI is relatively weak at 3 km resolution in Senegal. It is possible that cloud formation and vertical transport processes are already sufficiently represented by the model's resolved dynamics and microphysics, thus reducing the added value of parameterized shallow convection schemes.

In addition, the RRTMG_AERO experiment scheme exhibits the best performance for GHI at the two stations. The RRTMG_AERO_shallow experiment achieves the highest correlation coefficient (0.85), IOA (0.84), and SS (0.17), with low values of RMSE (160 W/m^2) and MAE (110 W/m^2), indicating a strong positive correlation between the predicted and the observed GHI values. Similar performance has also been observed for the no shallow scheme, with a correlation coefficient (0.85), IOA (0.85), and SS (0.17), along with RMSE (158 W/m^2), and MAE (110 W/m^2). The Dudhia scheme follows the RRTMG_AERO scheme in terms of performance, while the RRTMG scheme exhibits the least performance among the evaluated experiments. This is consistent with the findings of Verbois et al. (2018), who demonstrated that the Dudhia scheme outperforms RRTMG in solar irradiance forecasting. Moreover, the analysis has revealed a substantial difference in the metrics between the RRTMG and RRTMG_AERO schemes. The inclusion of aerosol effects improves the accuracy of the modelled GHI. Aerosols modify the intensity and distribution of radiation reaching the Earth's surface by absorbing and scattering solar radiation. By accounting for these effects, the integrated WRF-Solar model that incorporates aerosol data can provide a more accurate estimate of GHI over a given region. These results align with those reported by Sawadogo et al. (2023), who revealed that incorporating aerosol data that varies over time into the model enhanced the estimated GHI in West Africa. Jimenez et al. (2016) likewise demonstrated that the fully coupled WRF-Solar model reduced the biases in GHI estimation. Therefore, aerosol-radiation-cloud feedback can significantly improve the estimated GHI, particularly in regions with significant aerosol concentrations.

3.1.2 Seasonal performance of the GHI simulations

Figure 4 presents the seasonal performance analysis between observed GHI and the GHI estimates generated by the WRF-Solar model. RRTMG_AERO performs best

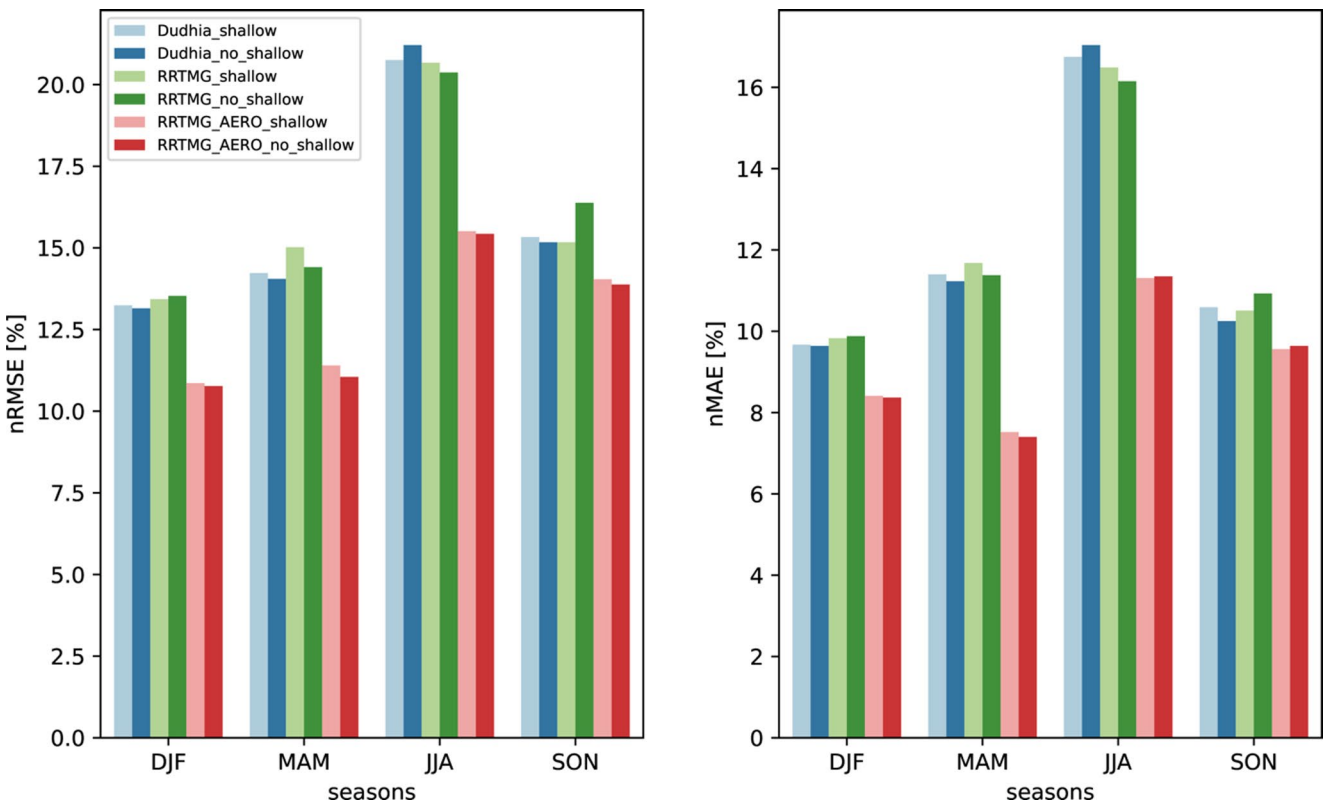

Fig. 4 Seasonal performance of WRF-Solar: the simulated GHI across various model experiments and both stations are evaluated using nRMSE and nMAE

in all seasons for both shallow and no-shallow schemes. Again, the activation of the shallow convection scheme in the WRF-Solar is weak throughout the season. The simulations using the Dudhia and RRTMG schemes show similar performance across all seasons, with only a tiny difference. However, in December-January-February (DJF), March-April-May (MAM), and September-October-November (SON) seasons, the Dudhia scheme, both shallow and no shallow, displays slightly better performance as compared to RRTMG, this is indicated by the relatively lower nRMSE and nMAE values. During DJF and MAM seasons, the values of nRMSE and nMAE are relatively low compared to the other seasons, indicating good performance. In June-July-August (JJA), the simulations show high values of nRMSE, with significantly high nMAE values. The climate pattern of the country may account for the reduced accuracy of WRF-Solar in estimating GHI in JJA. The rainy season occurs in JJA, hence the presence of clouds in this season. This underscores the difficulty of the model in estimating cloud properties.

This limitation of WRF-Solar to properly forecast cloud conditions is also discussed by Liu et al. (2022), who found that factors associated with entrainment and the cloud condensation threshold account for most of the variability in the ensemble simulations, especially in environments with lower pollution levels. According to Tapakis and Charalambides (2013), the quantity of irradiance reaching the Earth is significantly influenced by cloud cover, which is considered one of the most unpredictable variables. The results of this study align with the observations made by Sawadogo et al. (2023), who noted a substantial disparity in the hourly GHI estimates during the JJA season compared to other seasons.

3.1.3 Diurnal cycle performance of the GHI simulations

The performance of the model in the diurnal cycle (clear sky, cloudy sky, and high AOD) is also evaluated. Evaluation of the model's performance during clear sky is essential because clear sky conditions often serve as a baseline for estimating solar energy potential. The cloudy sky conditions help determine the model's capability to simulate cloud cover accurately and estimate the associated reduction in solar radiation. The high AOD conditions help assess its capability to account for aerosol effects and predict the resulting reduction in GHI. This is particularly important in regions with significant aerosols. This evaluation helps identify the model's potential biases, strengths, and limitations that could enable improvements in its parameterizations or input data.

3.1.3.1 The model's performance under clear sky The daily pattern of GHI for the different experiments and observations at Diass and Ten Merina under clear sky conditions is displayed in Fig. 5. The figure illustrates a comparison of the accuracy of different WRF-Solar con-

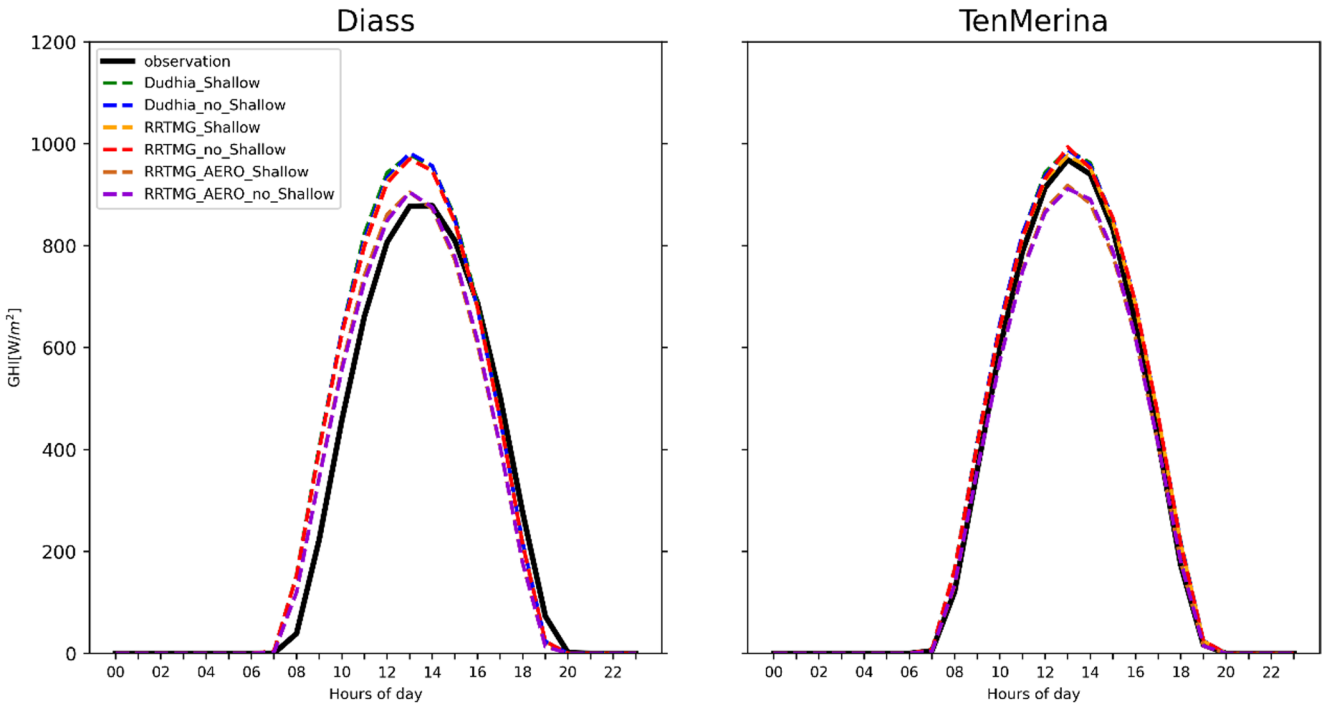

Fig. 5 Yearly average diurnal cycle of observed GHI at the two stations, along with simulated GHI from the various WRF Solar experiments under clear-sky situations

figurations considered in this study in reproducing the observed yearly average diurnal variation of GHI at the two stations. The performance of the experiments differs in Diass and Ten Merina. In TenMerina, the various experiments exhibit a better performance as they not only capture the diurnal variation but also the amplitude of the GHI. However, the RRTMG_AERO experiment fails to capture the peak of the observed GHI. On the other hand, in Diass, RRTMG_AERO well captures the peak of the observed GHI, whereas the other experiments overestimate it. Additionally, all experiments exhibit a temporal shift in the morning hours and align more closely with observations as the day progresses. This suggests that the impact of aerosol-radiation feedback, as represented in the RRTMG_AERO configuration, varies between the two sites, potentially due to differences in local aerosol loading despite their proximity (Fig. 6). The discrepancy of the performance in both sites could also be the bias in the CAMS aerosol data since the model incorporates the aerosol data directly into the radiative transfer routine without parametrization (Ruiz-Arias 2020). Moreover, the difference may arise from variations in aerosol concentration between the two stations under clear sky conditions, despite their proximity (Appendix B). Despite these differences, all experiments consistently reproduce the general pattern of the diurnal GHI cycle under clear-sky conditions, demonstrating the capability of WRF-Solar to simulate solar irradiance in cloud-free environments.

3.1.3.2 Performance of the model under cloudy sky Figure 7 displays the yearly average diurnal fluctuation of GHI, calculated from a compilation of cloudy days across the stations. In comparison to the effectiveness of WRF-Solar experiments on clear sky days, it is noteworthy that the model's performance is significantly lower under cloudy sky conditions at both stations. The different experiments generally fail to capture both the diurnal variability and the magnitude of the observed GHI, with a systematic overestimation at both locations.

One potential explanation for the lower performance of WRF-Solar under cloudy skies could be an underestimation of cloud features and properties within the model (Yang et al. 2021). Additionally, the timing of cloud occurrence might be inaccurate in the model simulations. This could lead to an incorrect representation of the intensity of GHI reaching the Earth's surface, as cloud cover diminishes the amount of

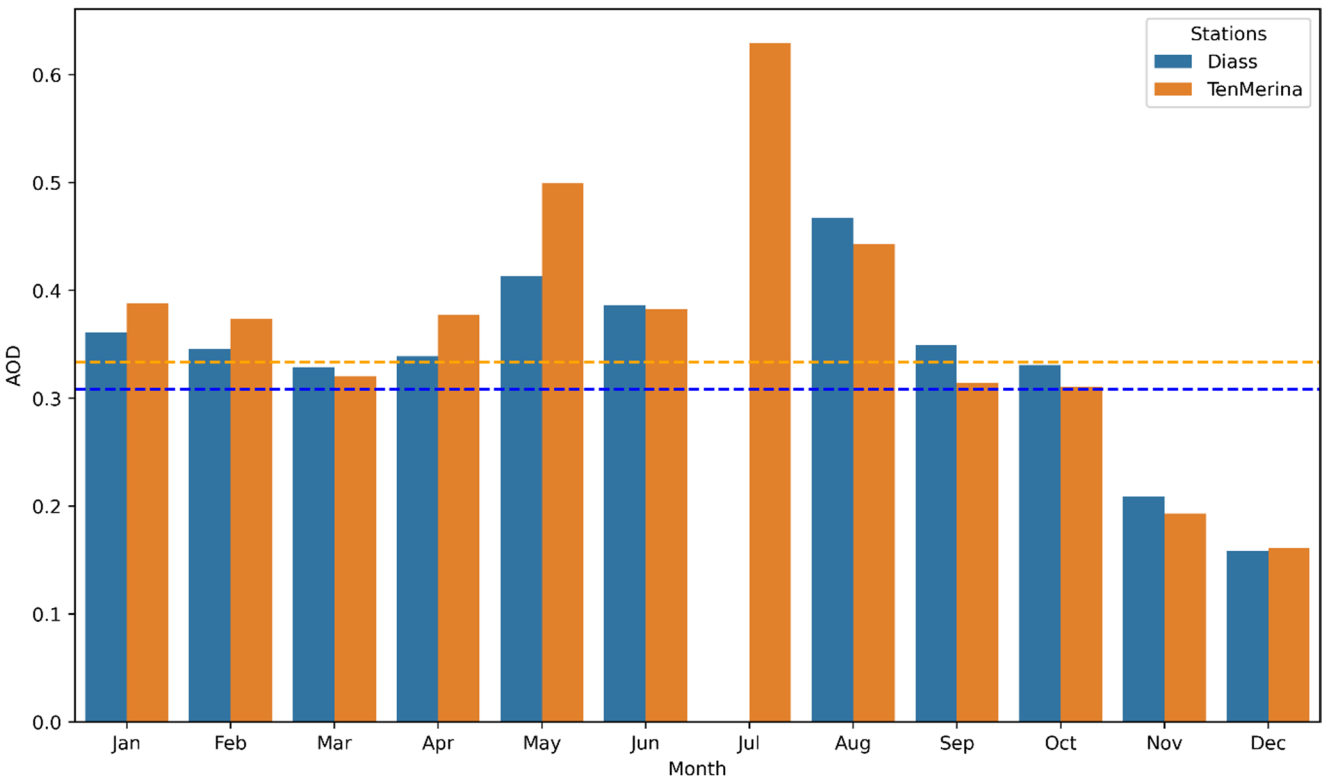

Fig. 6 Monthly AOD distribution over Ten Merina and Diass for 2020 under clear-sky conditions. The dashed orange and blue lines indicate the mean of the AOD in the two stations

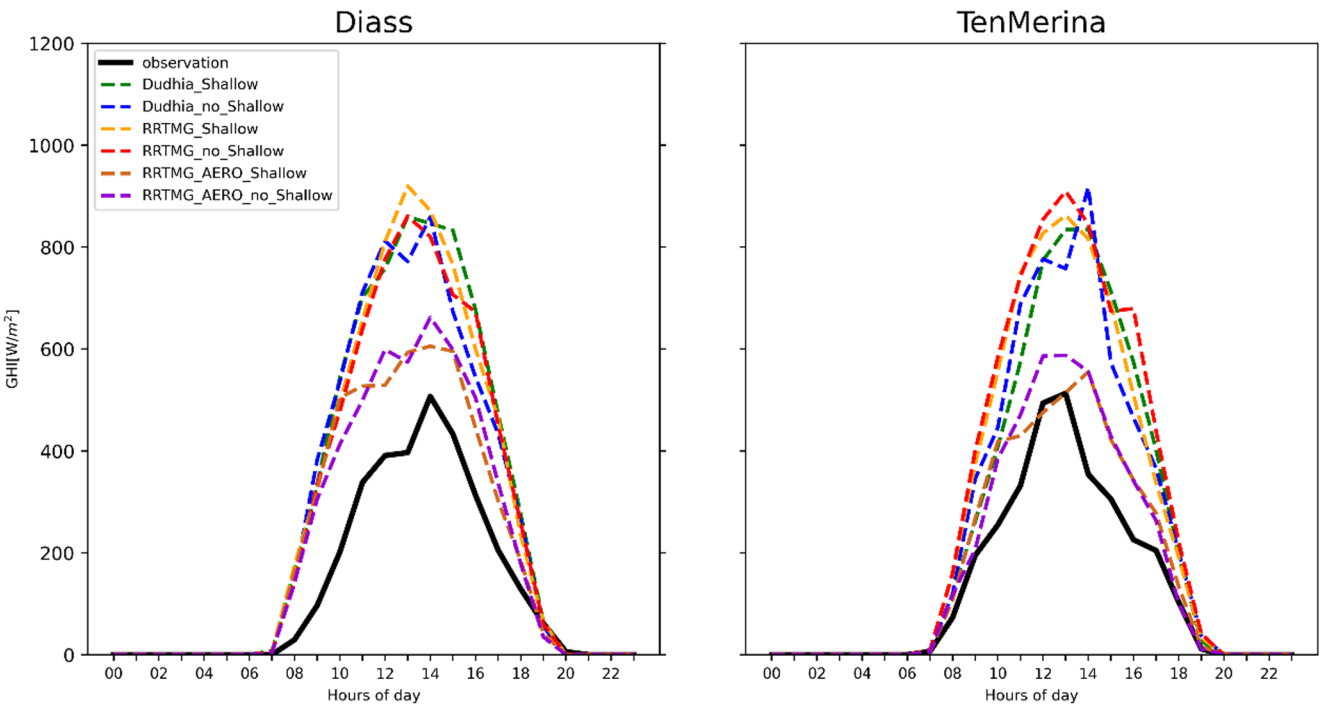

Fig. 7 Yearly average diurnal cycle of observed GHI at the two stations, along with simulated GHI from different WRF Solar experiments under cloudy-sky conditions

solar radiation that reaches the surface. The accuracy of the WRF model is affected by the choice of different physical parameterizations and numerical configurations. While previous studies have shown that the WRF-Solar model has effectively reduced biases in GHI compared to the standard WRF, substantial uncertainties remain in the model (Jimenez et al. 2016; Yang et al. 2021). Liu et al. (2022) demonstrated that three cloud-related variables - relative humidity near cloud base (RHa), relative humidity near cloud top (RHc), and the entrainment rate explain more than 80% of GHI variability under cloudy skies, highlighting the critical role of cloud microphysics. Moreover, uncertainties could also be related to aerosols, as they are present even on cloudy days. GHI has a high sensitivity to uncertainties in aerosol, albedo, and cloud properties in cloudy skies (Yang et al. 2021). The Thompson-Eidhammer microphysics scheme, which accounts for aerosol effects used in the RRTMG_AERO experiment, explicitly accounts for direct radiation-cloud-aerosol effects. Despite the enhancement in the radiation-cloud-aerosol feedback in WRF-Solar, uncertainties arising from model-specific parameters associated with aerosol effects and external factors remain (Liu et al. 2022). Nevertheless, the RRTMG_AERO shallow and no shallow schemes exhibit relative improvement under cloudy conditions.

3.1.3.3 Sources of uncertainty under cloudy sky To understand the poor performance of the WRF Solar model under cloudy skies at the two locations, we further analyse the vertically integrated water vapor (WVP) as a diagnostic variable to investigate the sources of cloud-related uncertainty.

The diurnal cycle of WVP under cloudy conditions reveals systematic differences across model configurations at both Diass and TenMerina (Fig. 8). RRTMG-based configurations consistently simulate higher column moisture (~47–49 kg m^{-2} at Diass and ~43–45 kg m^{-2} at TenMerina) compared to Dudhia-based schemes (~43–46 kg m^{-2} and ~40–42 kg m^{-2}, respectively), with the spread across configurations being more pronounced than the diurnal variability itself. A modest afternoon increase in WVP is evident across all configurations, driven by the diurnal growth of the convective boundary layer, which entrains surface moisture into the column as the mixed layer deepens in response to surface heating (Baldysz et al. 2024). The contrast between shallow and no-shallow convection runs further confirms that parameterized vertical moisture transport modulates boundary-layer humidity by controlling the vertical redistribution of moisture between the sub-cloud layer and the lower free troposphere. Despite

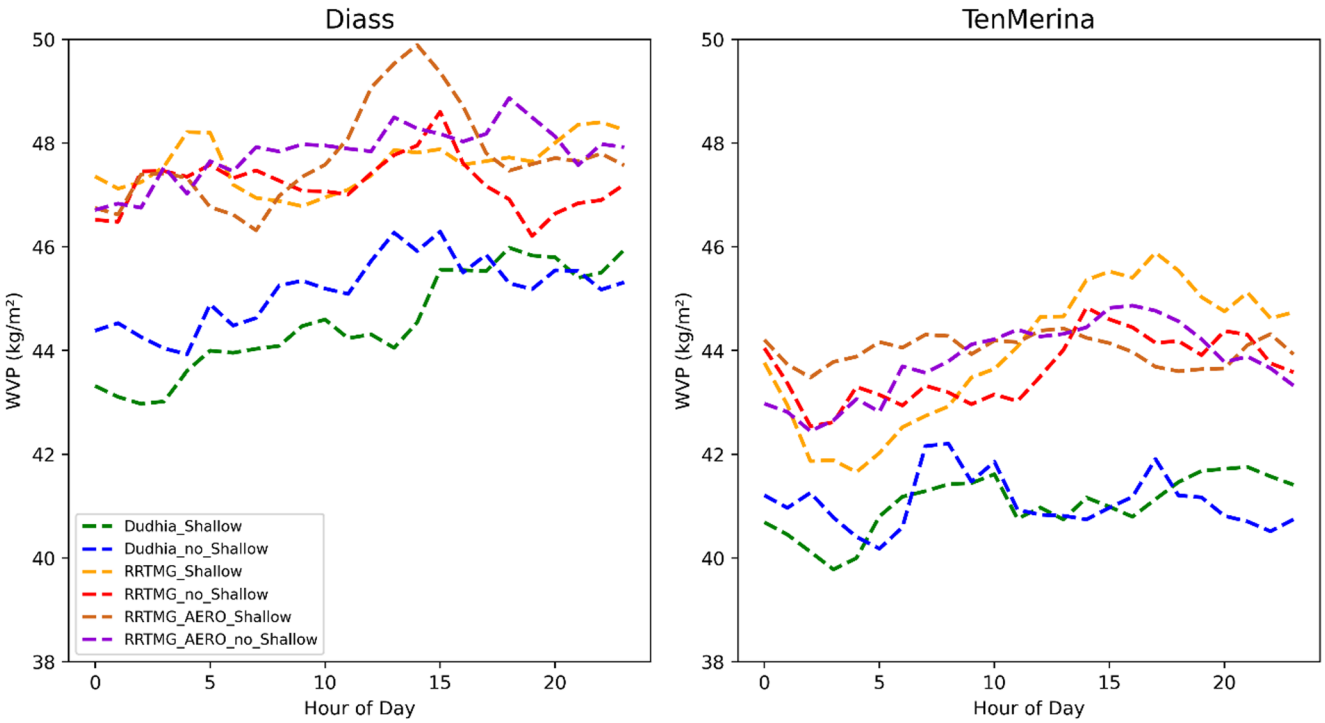

Fig. 8 Average diurnal cycle of water vapor under cloudy sky and at the two stations

this higher column moisture, all RRTMG-based configurations still exhibit a large positive GHI bias under cloudy sky (Fig. 7), with simulated GHI exceeding observations by up to ~300–400 W m^{-2} at peak. This indicates that the key uncertainty lies not in total moisture availability, but in how water vapor is converted into cloud liquid water, and in how cloud optical properties are represented within the radiation scheme (Thompson et al. 2016). Differences in column humidity alter cloud condensate production and optical thickness, and these effects propagate through cloud-radiation feedback, contributing to the systematic overestimation of surface irradiance under overcast conditions (Shan et al. 2022; Sawadogo et al. 2023; Song et al. 2021).

3.1.3.4 Performance of the model for high AOD Figure 9 shows the average daily variation of GHI, computed from a compilation of days characterized by high AOD across the stations. The WRF experiments exhibit improved performance on days characterized by low AOD values of 0.1 at both stations. During such conditions, the model effectively captures the amplitude and variations of GHI, albeit with a slight underestimation at the Ten Merina station. In comparison, the RRTMG and Dudhia radiation schemes, whether considering a shallow convection scheme or not, slightly demonstrate a closer approximation to the observed GHI amplitude than the RRTMG_AERO scheme.

Conversely, on days characterized by high AOD (2.2 and 2.3), respectively, at Ten Merina and Diass, the RRTMG_AERO scheme, including both shallow and non-shallow configurations, demonstrates better performance in representing GHI with a closer amplitude to the observed GHI. In these situations, the RRTMG_AERO proves to be more effective in capturing the variations and magnitude of GHI than other schemes. Importantly, the shallow convection scheme makes almost no contribution under these high-AOD conditions, indicating that the shallow convection scheme has a negligible role in representing GHI under high-AOD conditions.

The inclusion of aerosol effects in the RRTMG_AERO scheme contributes to a more accurate representation of GHI under such high AOD conditions. This finding aligns with the study by Sosa-Tinoco et al. (2022), who demonstrated that incorporating AOD into the WRF-Solar simulations reduces the MAE of predicted solar irradiance by 10.9% compared to runs without AOD, particularly under high aerosol conditions. Nonetheless, despite efforts to account for aerosol effects in the RRTMG_AERO scheme, it is essential to acknowledge that uncertainties remain. This is consistent with the results found in the diurnal

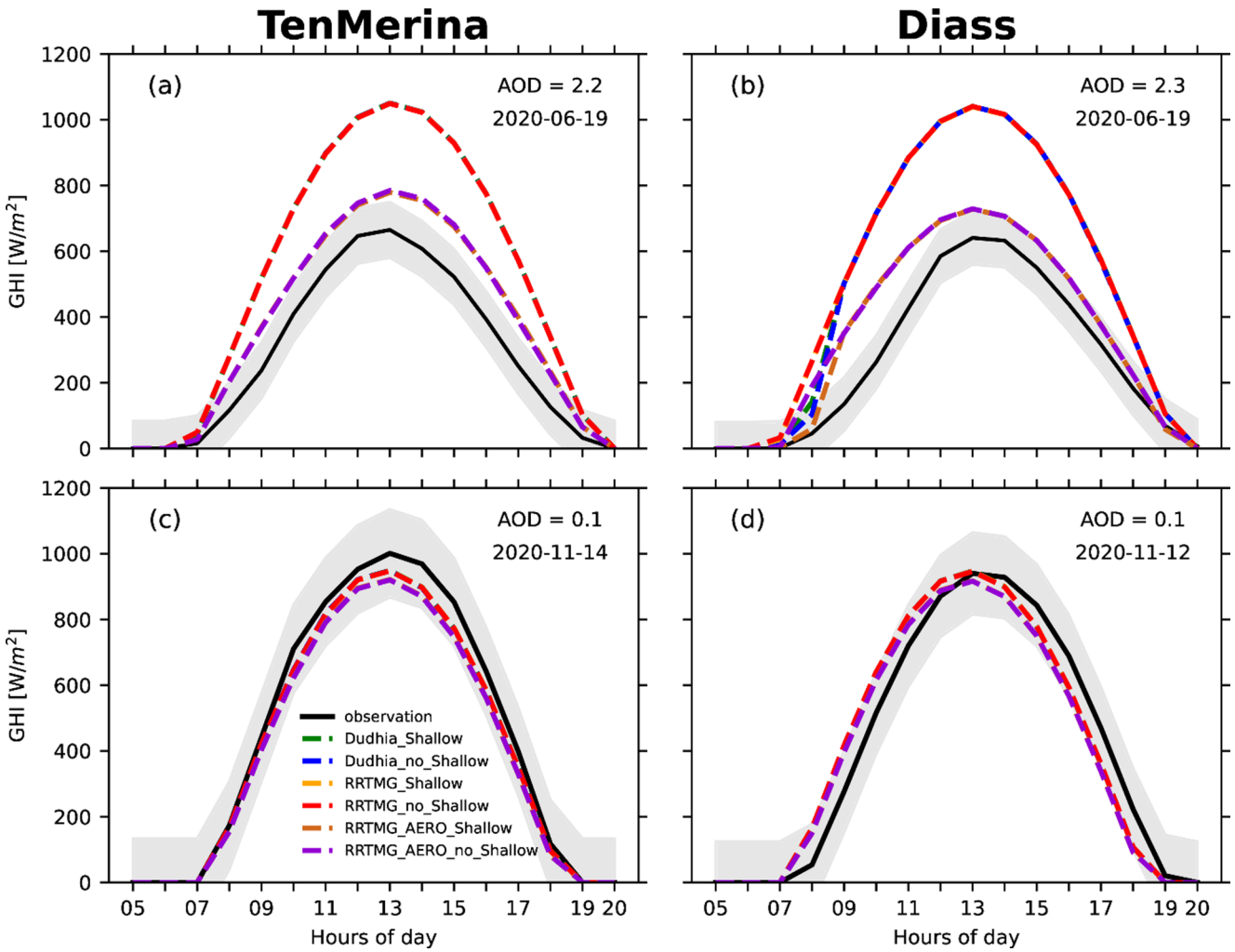

Fig. 9 Diurnal variation of observed and simulated GHI at the two stations under high AOD situations

pattern of GHI in Ten Merina under clear skies (Fig. 5) when the RRTMG_AERO experiments fail to accurately reproduce the maximum of the observation. Therefore, further research and improvements in the assimilation of aerosol processes are necessary to enhance the precision of GHI predictions in WRF-Solar. Overall, the inclusion of a shallow convection scheme appears to have a minimal contribution to the representation of the GHI under high AOD.

3.1.4 Overall performance

Table 3 provides an overview of the performance of the various experiments for the two stations under clear and cloudy days. The statistical results from the metrics indicate that the model is quite effective in estimating GHI at both locations. The model's simulations exhibit higher accuracy under clear sky conditions compared to cloudy skies. For Diass, under clear sky conditions, the average correlation coefficient is 0.91, with a SS of 0.25, a RMSE of 135 W/m^2, and a MAE of 108 W/m^2. On the other hand, under cloudy conditions, the correlation and the SS drop to 0.6 and −1.19, and the corresponding RMSE and MAE values increase to 341 W/m^2 and 281 W/m^2, respectively. At the Ten Merina station, under clear sky conditions, the model shows better performance with an average correlation of 0.93 and SS of 0.42, along with a RMSE of 114.1 W/m^2, and a MAE of 77.9 W/m^2. Conversely, under cloudy sky conditions, the correlation and SS decrease to 0.58 and −0.9, and the RMSE and MAE values increase to 324.5 W/m^2 and 258.7 W/m^2, respectively. These findings highlight that the WRF-Solar model's forecasting accuracy for GHI highly depends on sky conditions at both locations.

Table 3 Error values for GHI forecasts(W/m^2) are categorized according to the prevailing sky conditions

Sky Conditions	Station	RMSE	nRMSE	*R*	MAE	nMAE	IAO	SS	Experiment	Best Experiment
Cloudy Sky	Diass	382	41.32	0.66	323.73	35.01	0.47	−1.45	Dudhia_Shallow	
	Diass	374	40.45	**0.68**	309.09	33.43	0.48	−1.4	RRTMG_Shallow	
	Diass	**263**	**28.45**	0.55	**209.13**	**22.62**	**0.6**	**−0.69**	RRTMG_AERO_Shallow	RRTMG_AERO_Shallow
	Diass	373	40.34	0.61	307.66	33.28	0.47	−1.4	Dudhia_no_Shallow	
	Diass	386	41.75	0.55	316.98	34.28	0.46	−1.48	RRTMG_no_Shallow	
	Diass	**268**	**28.99**	0.57	**219.33**	**23.72**	0.59	**−0.72**	RRTMG_AERO_no_Shallow	RRTMG_AERO_no_Shallow
	TenMerina	367	42.29	0.54	295.9	34.09	0.48	−1.15	Dudhia_Shallow	
	TenMerina	367	42.29	**0.64**	297.88	34.32	0.47	−1.15	RRTMG_Shallow	
	TenMerina	**245**	**28.23**	0.46	**182.13**	**20.99**	0.6	**−0.43**	RRTMG_AERO_Shallow	RRTMG_AERO_Shallow
	TenMerina	359	41.36	0.57	285.1	32.85	0.49	−1.1	Dudhia_no_Shallow	
	TenMerina	380	43.78	0.7	317.25	36.55	0.46	−1.23	RRTMG_no_Shallow	
	TenMerina	**229**	**26.39**	0.56	**174.24**	**20.08**	**0.64**	**−0.34**	RRTMG_AERO_no_Shallow	RRTMG_AERO_no_Shallow
Clear Sky	Diass	138	14.01	**0.93**	114.17	11.59	0.87	0.23	Dudhia_Shallow	
	Diass	142	14.41	0.91	115.8	11.75	0.87	0.21	RRTMG_Shallow	
	Diass	**122**	**12.38**	0.9	**93.48**	**9.49**	**0.89**	**0.32**	RRTMG_AERO_Shallow	RRTMG_AERO_Shallow
	Diass	141	14.31	0.92	115.62	11.73	0.87	0.22	Dudhia_no_Shallow	
	Diass	145	14.72	0.9	116.86	11.86	0.86	0.2	RRTMG_no_Shallow	
	Diass	**122**	**12.38**	0.9	**93.37**	**9.48**	**0.89**	**0.32**	RRTMG_AERO_no_Shallow	RRTMG_AERO_no_Shallow
	TenMerina	113	9.22	**0.94**	81.12	6.62	0.91	0.43	Dudhia_Shallow	Dudhia_Shallow
	TenMerina	119	9.71	0.93	82.62	6.74	0.91	0.4	RRTMG_Shallow	
	TenMerina	114	9.3	0.93	**72.02**	**5.88**	0.91	0.43	RRTMG_AERO_Shallow	RRTMG_AERO_Shallow
	TenMerina	**112**	**9.14**	**0.94**	79.63	6.5	0.91	**0.44**	Dudhia_no_Shallow	Dudhia_no_Shallow
	TenMerina	115	9.38	0.93	80.35	6.56	0.91	0.42	RRTMG_no_Shallow	
	TenMerina	**112**	**9.14**	0.93	**72.18**	**5.89**	0.91	**0.44**	RRTMG_AERO_no_Shallow	RRTMG_AERO_no_Shallow

Additionally, the results indicate that under clear sky conditions in Diass, the RRTMG_AERO experiment, both with and without considering a shallow convection scheme, demonstrates better performance in estimating GHI. Following that, the Dudhia scheme also showed relatively good performance. Similarly, in Ten Merina, RRTMG_AERO and the Dudhia simulations exhibit the most accurate GHI estimates. Nevertheless, when considering the MAE, the RRTMG_AERO scheme performs best. This aligns with the study of Sawadogo et al. (2023), who found that RRTMG_AERO and Dudhia schemes are the best in estimating GHI for 18 stations in West Africa (Ghana and Burkina). Although their study area is in the Guinea and Savannah zones, both regions are influenced by Saharan dust and biomass-burning aerosols, which are also key aerosol sources in the Sahel. This similarity in aerosol characteristics may partly explain the performance of the two radiation schemes across these regions.

Under cloudy conditions in both stations, all experiments show a significant uncertainty in GHI estimation. This corresponds with earlier studies (Yang et al. 2021; Liu et al. 2022), which indicate that the WRF-Solar model has uncertainties in GHI estimation on cloudy days. Nonetheless, the RRTMG_AERO experiment remains the best-performing scheme for forecasting GHI. This experiment consistently outperforms other schemes in accurately capturing GHI. This indicates the experiment's effectiveness in accounting for aerosol effects and its ability to provide reliable GHI predictions, even though some improvements are required.

These findings suggest that in both stations, the RRTMG_AERO scheme, with its inclusion of aerosol effects, shows favourable performance for GHI estimation under clear and cloudy skies. The Dudhia scheme also performs well, although the RRTMG_AERO scheme outperforms it when considering MAE.

On the other hand, the effect of shallow convection scheme in WRF-Solar has a minimal impact on the estimated GHI at both stations under clear skies. This is evident in Fig. 10, where during the dry season (JFM), which consists predominantly of clear-sky days, there is minimal variation in the total cloudiness across the two simulations. The limited sensitivity to shallow convection can partly be explained by the 3 km grid spacing, at which a portion of shallow convection processes is already resolved explicitly by the model dynamics, thereby

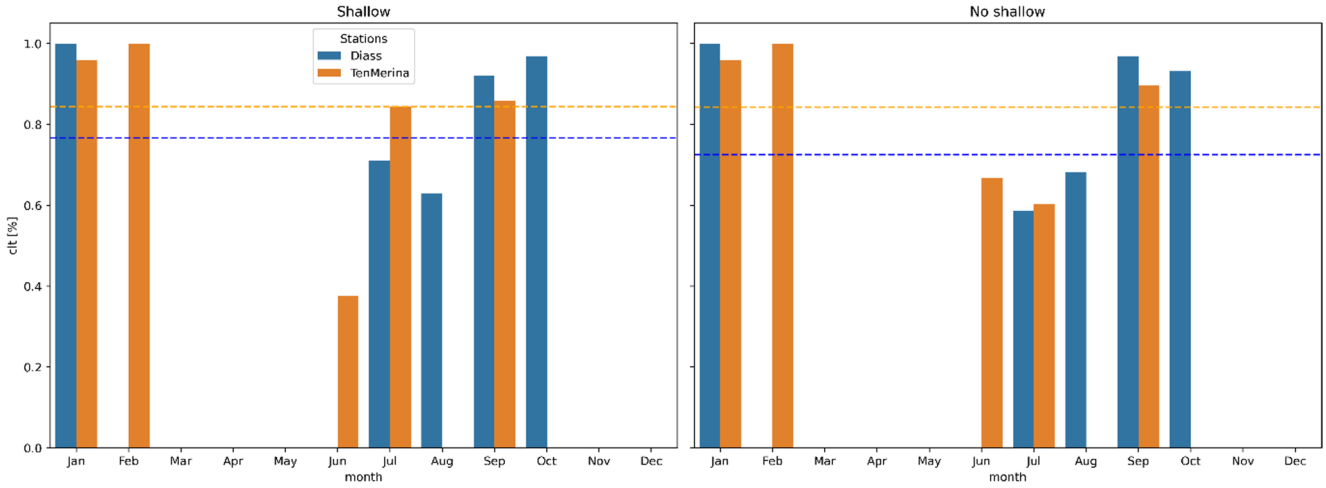

Fig. 10 Difference of daily total cloud cover between shallow and no_shallow with the RRTMG_AERO experiment in Diass and Ten Merina for the year 2020

reducing the added value of a parameterized shallow convection scheme.

Nonetheless, during the rainy season, which is characterized by a higher incidence of cloudy days, there are some differences in total cloud cover between the shallow and no shallow experiments. Both stations show a similar monthly value of total cloud cover but with a difference in the JJA season. In the West African monsoon regime, deep convection plays a dominant role in cloud formation and radiative variability, which may further explain why shallow convection parameterization exerts only little influence compared to regions where shallow cumulus clouds are more prevalent.

Despite that, in Ten Merina, the difference in terms of RMSE between the shallow and no shallow experiment is higher with the RRTMG_AERO experiment (16 W/m^2) compared to Diass (5 W/m^2). This inland response may reflect enhanced land-atmosphere coupling and boundary-layer turbulence, which can modulate low-level cloud development and thermodynamic profiles. This allows shallow convection parameterizations to exert a more noticeable though still limited impact on radiation. Additionally, the cloud properties produced by the shallow scheme may contain substantial biases (Zhang and Bretherton 2008). These biases can be further compounded by uncertainties related to aerosol-radiation-cloud feedback in the model, particularly due to inaccuracies in aerosol input data. Previous studies have shown that the AOD from CAMS reanalysis has bias during high aerosol concentration in West Africa compared to in situ data (Léon et al. 2021). This indicates that the inherent bias from aerosol into the model may result in a high bias in GHI estimates over the region when Deng's shallow convection scheme is turned on.

In contrast, when the model excludes aerosol input, RRMTG coupled with the shallow convection scheme performs slightly better than without it. For instance, in Ten Merina, this configuration improves the GHI estimates by about 2% in terms of MAE. Nevertheless, simulations that include aerosol information generally provide more accurate GHI estimates across all atmospheric conditions. Overall, the activation of shallow convection has a weak impact on the GHI estimation over Senegal under all atmospheric conditions.

4 Summary and conclusions

The study investigated the effectiveness of two shortwave radiation schemes, Dudhia and RRTMG, within the WRF-Solar model for two solar power plants in Senegal: Diass and Ten Merina. The simulations used a one-way, two-nested domain configuration, where the larger domain (West Africa) had a resolution of 15 km, and the inner domain (Senegal) had a resolution of 3 km, with the analysis centred on the latter. The experiments of WRF-Solar were evaluated using observed instantaneous hourly GHI from the solar plants for 2020. This is the first study to examine WRF-Solar's performance specifically for solar power plants operated by energy companies in West Africa. The RRTMG scheme was investigated in two simulations, one without considering AOD and one with

time-varying AOD (RRTMG_AERO). Additionally, the study explored the influence of shallow convection on all simulations.

The evaluation process involved examining the WRF-Solar model's effectiveness under different sky conditions, including all-sky, clear-sky, cloudy situations, and high AOD. By considering GHI measurements from these diverse sky conditions, a comprehensive analysis of the model's performance and its capability to capture the variations in solar irradiance across diverse atmospheric conditions was achieved. The key findings can be outlined as follows:

- For the seasonal evaluation of the model, it is observed that the nRMSE and nMAE are relatively low for DJF and MAM compared to the other seasons, indicating good performance in these seasons. However, the JJA season showed the lowest performance of the experiments, characterized by high values of nRMSE and nMAE.
- Under clear sky, the model simulations successfully replicate the daily pattern and magnitude of the observations, even though there is a slight underestimation at Ten Merina from RRTMG_AERO. In contrast, the model's performance is noticeably diminished under cloudy sky conditions at both stations, as cloud cover causes challenges in accurately predicting irradiance.
- Under high AOD conditions, the experiments are observed to be better on days characterized by low AOD values rather than high values.
- Overall, the RRTMG_AERO scheme, regardless of the consideration of the shallow convection scheme, exhibits superior performance in forecasting GHI at these stations. This is followed by the Dudhia scheme, which also shows relatively good performance.
- The shallow convection scheme in the WRF-Solar model exhibited a minimal impact on GHI estimation across different atmospheric conditions at both locations.

The results suggest that the impact of including shallow clouds in the model doesn't significantly enhance its ability to forecast GHI at the studied stations. However, there are some slight differences under cloudy skies in Ten Merina. To better understand the impact of including shallow clouds in the model over West Africa, using sub-hourly data, as done by Jiménez et al. (2022), would provide more detailed insights. Using sub-hourly data would allow to capture rapid changes in cloud cover and solar irradiance. Further investigation using sub-hourly data in the West African context could provide a deeper insight into the impact of shallow clouds on solar irradiance estimation.

These findings highlight the performance of various radiation schemes in WRF-Solar for forecasting GHI at the Diass and Ten Merina solar plants in Senegal. The results indicate that the RRTMG_AERO scheme performs better than other schemes. This applies to clear, cloudy, and all-sky conditions. Moreover, they emphasize the significance of selecting appropriate radiation schemes and considering aerosol effects in GHI forecasting models while also showing the relatively minor role of the shallow scheme in improving GHI representation. Nevertheless, it is crucial to acknowledge that the model still exhibits significant biases, particularly under cloudy sky conditions. This indicates the challenge of accurately simulating GHI under such conditions in Senegal. The same challenge is noticed in other regions. While there is improvement in the model, biases remain especially under cloudy sky. Future research should focus on improving the representation of cloud processes in WRF solar, as this remains a key source of uncertainty in GHI estimation. Consequently, further adaptation and development of the WRF-Solar model, particularly in improving aerosol-cloud-radiation feedback, are essential to improve GHI forecasting accuracy.

These findings have practical implications for solar energy development and grid management in Senegal. The superior performance of the RRTMG_AERO scheme suggests that incorporating time-varying aerosol information into WRF-Solar can enhance the accuracy of solar irradiance forecasts. Given the growing penetration of solar energy in Senegal's energy mix, WRF-Solar forecasts could support plant managers particularly during the dry season (October-May), which is dominated by clear-sky days. In the rainy season, more accurate GHI forecasts are essential for scheduling and maintaining grid stability. Our results indicate that operational forecasts in Senegal would benefit from adopting RRTMG_AERO as the default configuration. This provides energy planners and utilities with a pathway for using WRF-Solar as a practical forecasting tool to support the growing renewable energy sector in the country.

Appendix A. Performance of the model under cloudy days

This annex shows the model's performance under cloudy-sky conditions, focusing on selected examples rather than annual averages. As shown and discussed in Sect. 3.1.3.2, which presents the diurnal cycle of the annual average for cloudy days at each site, all experiments fail to reproduce both the diurnal variation and the magnitude of GHI. Moreover, GHI is consistently overestimated at both stations.

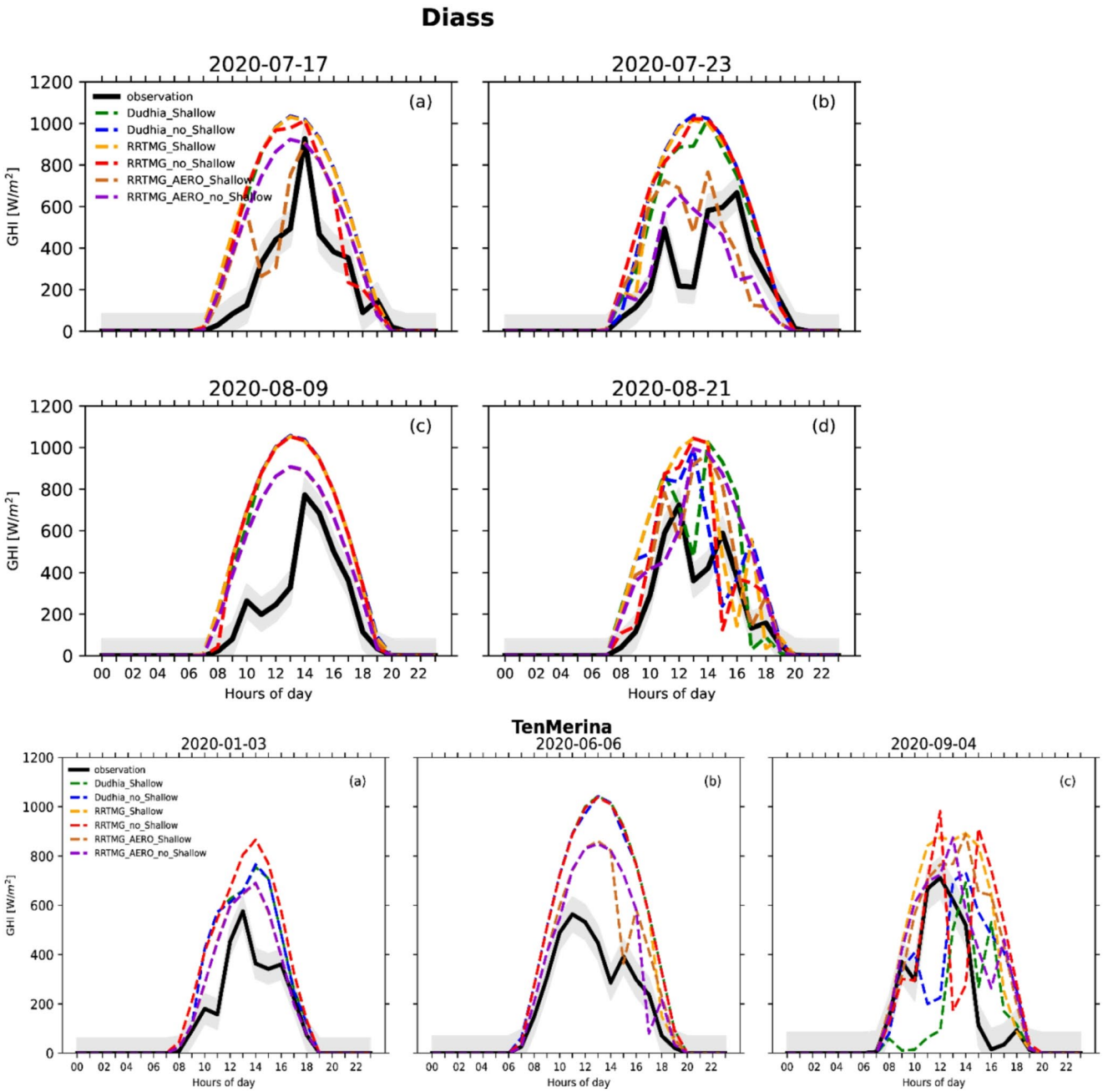

Fig. 11 Diurnal variation of GHI for the WRF-Solar configurations and observations at the two stations under cloudy-sky conditions

Appendix B. Mean spatial distribution of AOD over senegal

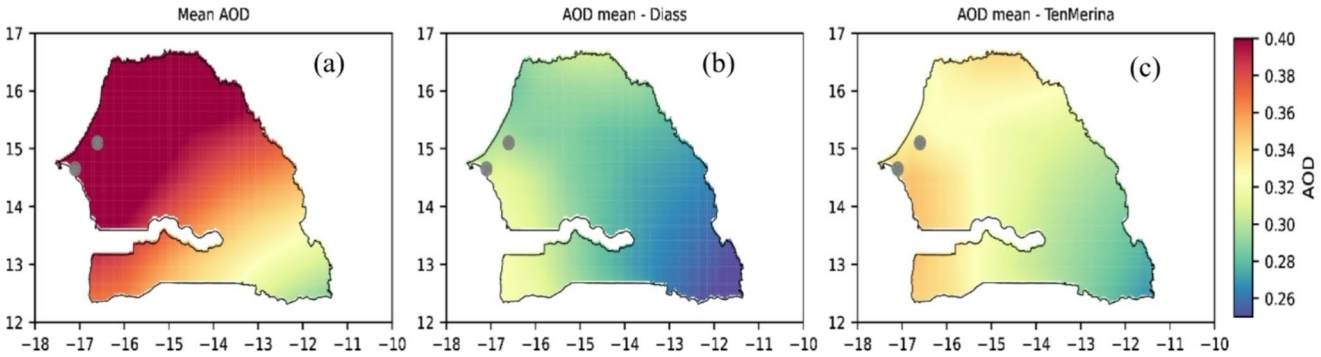

Fig. 12 (**a**) Annual mean spatial distribution of AOD over Senegal. (**b**) Annual mean spatial distribution of AOD over Senegal, considering only clear sky days in Diass. (**c**) Annual mean spatial distribution of AOD over Senegal, considering only clear sky days in TenMerina.

Acknowledgements We extend our gratitude to ECMWF and CAMS for granting access to their datasets used in this study.

Author contributions AN: Writing original draft, Review & editing, Visualization, Software, Methodology, Funding acquisition, Conceptualization. WS: Review & editing, Software, Methodology. JB: Review & editing, Methodology, SupervisionCD: Review & editing, Supervision. MSM: Review & editing, Supervision. ATG: Review & editing, Supervision. HK: Review & editing, Supervision, Resources.

Funding Open Access funding enabled and organized by Projekt DEAL. This publication was made possible with the financial support of the German Ministry for Education and Research (BMBF) through the West African Science Service Center on Climate Change and Adapted Land Use (WASCAL), the Prince Albert II of Monaco Foundation (IPCC scholarship - Sixth Round of Awards), and the Alexander von Humboldt Foundation through the International Climate Protection Fellowship. The content of this document is solely the responsibility of Aissatou Ndiaye and does not necessarily reflect the views of these foundations and programs.

Data availability The observed data from the solar plants used in this study are not accessible to the public. The ERA5 data can be downloaded at [https://www.ecmwf.int//en/forecasts/datasets/reanalysis-datasets/era5](https:/www.ecmwf.int/en/forecasts/datasets/reanalysis-datasets/era5). The WRF source code is available for download at [https://github.com/wrf-model/WRF/archive/refs/tags/v4.2.2.zip](https:/github.com/wrf-model/WRF/archive/refs/tags/v4.2.2.zip).

Declarations

Competing interests The authors declare no competing interests.

References

Abdallah AA, Eid MM, Wahab MMA, El-Hussainy FM (2015) Regional Climate Simulation of WRF Model over North Africa: Temperature and Precipitation. World Environ 5(4):160–173. https://doi.org/10.5923/j.env.20150504.04

Arbizu-Barrena C, Ruiz-Arias JA, Rodríguez-Benítez FJ, Pozo-Vázquez D, Tovar-Pescador J (2017) Short-term solar radiation forecasting by advecting and diffusing MSG cloud index. Sol Energy 155:1092–1103. https://doi.org/10.1016/j.solener.2017.07.045

Arnault J, Knoche R, Wei J, Kunstmann H (2016) Evaporation tagging and atmospheric water budget analysis with WRF: A regional precipitation recycling study for West Africa. Water Resour Res 52(3):1544–1567. https://doi.org/10.1002/2015WR017704

Aryaputera AW, Yang D, Walsh WM (2015) Day-Ahead Solar Irradiance Forecasting in a Tropical Environment. J Solar Energy Eng Trans ASME 137(5). https://doi.org/10.1115/1.4030231

Baldysz Z, Nykiel G, Baranowski DB, Latos B, Figurski M (2024) Diurnal variability of atmospheric water vapour, precipitation and cloud top temperature across the global tropics derived from satellite observations and GNSS technique. Clim Dyn 62(3):1965–1982. https://doi.org/10.1007/s00382-023-07005-0

Benitez IB, Ibañez JA, Lumabad CIIID, Cañete JM, Principe JA (2023) Day-ahead hourly solar photovoltaic output forecasting using SARIMAX, long short-term memory, and extreme gradient boosting: case of the Philippines. Energies. https://doi.org/10.3390/en16237823

Bliefernicht J, Berger S, Salack S, Guug S, Hingerl L, Heinzeller D, Mauder M, Steinbrecher R, Steup G, Bossa AY, Waongo M, Quansah E, Balogun AA, Yira Y, Arnault J, Wagner S, Klein C, Gessner U, Knauer K, Kunstmann H (2018) The WASCAL Hydrometeorological Observatory in the Sudan Savanna of

Burkina Faso and Ghana. Vadose Zone J 17(1):1–20. https://doi.org/10.2136/vzj2018.03.0065

BSRN (2021) Baseline surface radiation network. World Radiation Monitoring Center. https://bsrn.awi.de/

Chen F, Dudhia J (2001) Coupling an advanced land surface-hydrology model with the Penn State-NCAR MM5 Modeling System. Part I: Model Implementation and Sensitivity

Danso DK, Anquetin S, Diedhiou A, Kouadio K, Kobea AT (2020) Daytime low-level clouds in West Africa – occurrence, associated drivers, and shortwave radiation attenuation. Earth Syst Dynam 11:1133–1152. https://doi.org/10.5194/esd-11-1133-2020

Deng A, Gaudet B, Dudhia J, Kiran Alapaty AND (2014) Implementation & Evaluation of a New Shallow Convection Scheme in WRF. In Proceedings, 94th AMC 26th Conference, Atlanta, GA, February 02–06, 2014. American Meteorological Society, Boston, MA, 12.5

Diaz JP, González A, Expósito FJ, Pérez JC, Fernández J, García-Díez M, Taima D (2015) WRF multi-physics simulation of clouds in the African region. Q J R Meteorol Soc 141(692):2737–2749. https://doi.org/10.1002/qj.2560

Dinku T (2019) Challenges with availability and quality of climate data in Africa. In Extreme Hydrology and Climate Variability: Monitoring, Modelling, Adaptation and Mitigation (pp. 71–80). Elsevier. https://doi.org/10.1016/B978-0-12-815998-9.00007-5

Diokhane AM, Jenkins GS, Manga N, Drame MS, Mbodji B (2016) Linkages between observed, modeled Saharan dust loading and meningitis in Senegal during 2012 and 2013. Int J Biometeorol 60(4):557–575. https://doi.org/10.1007/s00484-015-1051-5

D'Isidoro M, Briganti G, Vitali L, Righini G, Adani M, Guarnieri G, Moretti L, Raliselo M, Mahahabisa M, Ciancarella L, Zanini G, Fino E (2020) Estimation of solar and wind energy resources over Lesotho and their complementarity by means of WRF yearly simulation at high resolution. Renewable Energy 158:114–129. https://doi.org/10.1016/j.renene.2020.05.106

Fall S, Niyogi D, Mohanty UC, Kumar A (2007) Application of weather prediction models for hazard mitigation planning: A case study of heavy off-season rains in Senegal. Nat Hazards 41(1):227–243. https://doi.org/10.1007/s11069-006-9033-x

Gamarro H, Gonzalez JE, Ortiz LE (2019) On the assessment of a numerical weather prediction model for solar photovoltaic power forecasts in cities. J Energy Resour Technol Trans ASME 141(6). https://doi.org/10.1115/1.4042972

Garrigues S, Remy S, Chimot J, Ades M, Inness A, Flemming J, Kipling Z, Laszlo I, Benedetti A, Ribas R, Jafariserajehlou S, Fougnie B, Kondragunta S, Engelen R, Peuch V-H, Parrington M, Bousserez N, Vazquez Navarro M, Agusti-Panareda A (2022) Monitoring multiple satellite aerosol optical depth (AOD) products within the Copernicus Atmosphere Monitoring Service (CAMS) data assimilation system. Atmos Chem Phys 22(22):14657–14692. https://doi.org/10.5194/acp-22-14657-2022

Gavina CJA, Ibañez JA, Benitez IB, Lumabad CD, Principe JA (2024) ASSESSMENT OF REANALYSIS DATA FOR SOLAR PV OUTPUT FORECASTING IN THE PHILIPPINES: CASE OF PANGASINAN, NEGROS OCCIDENTAL, AND DAVAO DEL NORTE. Int Archives Photogrammetry Remote Sens Spat Inform Sci - ISPRS Archives 484/W8–2023:279–284. https://doi.org/10.5194/isprs-archives-XLVIII-4-W8-2023-279-2024

Gueymard C, Jimenez P (2019) Validation of Real-Time Solar Irradiance Simulations Over Kuwait Using WRF-Solar. 1–11. https://doi.org/10.18086/eurosun2018.09.14

Haupt SE, Kosovic B, Jensen T, Lee J, Jimenez P, Lazo J, Cowie J, Mccandless T, Pearson J, Weiner G, Alessandrini S, Monache LD, Yu D, Peng Z, Huang D, Heiser J, Yoo S, Kalb P, Miller S, Hinkleman L (2016) THE SUN4CAST® Solar power forecasting system: the results of the public-private-academic partnership to advance solar power forecasting NCAR/TN-526+STR NCAR technical note

Hersbach H, Bell B, Berrisford P, Hirahara S, Horányi A, Muñoz-Sabater J, Nicolas J, Peubey C, Radu R, Schepers D, Simmons A, Soci C, Abdalla S, Abellan X, Balsamo G, Bechtold P, Biavati G, Bidlot J, Bonavita M, Thépaut JN (2020) The ERA5 global reanalysis. Q J R Meteorol Soc 146(730):1999–2049. https://doi.org/10.1002/qj.3803

IRENA and AfDB (2022) Renewable Energy Market Analysis: Africa and Its Regions, International Renewable Energy Agency and African Development Bank, Abu Dhabi and Abidjan. Available for download: www.irena.org/publications

Jenkins GS, McCauley K, Thompson T, Diokhane AM (2022) WRF-CHEM simulations of unhealthy PM 10 concentrations during four dust events in Senegal. Journal of Geophysical Research: Atmospheres. https://doi.org/10.1029/2022JD037068

Jimenez PA, Hacker JP, Dudhia J, Haupt SE, Ruiz-Arias JA, Gueymard CA, Thompson G, Eidhammer T, Deng A (2016) WRF-SOLAR: Description and clear-sky assessment of an augmented NWP model for solar power prediction. Bull Am Meteorol Soc 97(7):1249–1264. https://doi.org/10.1175/BAMS-D-14-00279.1

Jiménez PA, Yang J, Kim JH, Sengupta M, Dudhia J (2022) Assessing the WRF-Solar Model Performance Using Satellite-Derived Irradiance from the National Solar Radiation Database. J Appl Meteorol Climatology 61(2):129–142. https://doi.org/10.1175/JAMC-D-21-0090.1

Klein C, Heinzeller D, Bliefernicht J, Kunstmann H (2015) Variability of West African monsoon patterns generated by a WRF multi-physics ensemble. Clim Dyn 45(9–10):2733–2755. https://doi.org/10.1007/s00382-015-2505-5

Knobelspiesse KD, Pietras C, Fargion GS, Wang M, Frouin R, Miller MA, Subramaniam A, Balch WM (2004) Maritime aerosol optical thickness measured by handheld sun photometers. Remote Sens Environ 93(1–2):87–106. https://doi.org/10.1016/j.rse.2004.06.018

Lara-Fanego V, Ruiz-Arias JA, Pozo-Vázquez D, Santos-Alamillos FJ, Tovar-Pescador J (2012) Evaluation of the WRF model solar irradiance forecasts in Andalusia (southern Spain). Solar Energy 86(8):2200–2217. https://doi.org/10.1016/j.solener.2011.02.014

Larson VE (2013) Forecasting Solar Irradiance with Numerical Weather Prediction Models. Solar Energy Forecasting and Resource Assessment. Elsevier Inc, pp 299–318. https://doi.org/10.1016/B978-0-12-397177-7.00012-7

Lee JA, Haupt SE, Jiménez PA, Rogers MA, Miller SD, McCandless TC (2017) Solar irradiance nowcasting case studies near sacramento. J Appl Meteorol Climatology 56(1):85–108. https://doi.org/10.1175/JAMC-D-16-0183.1

Liu Y, Qian Y, Feng S, Berg LK, Juliano TW, Jiménez PA, Liu Y (2022) *Sensitivity of solar irradiance to model parameters in cloud and aerosol treatments of WRF-Solar 2 3 4*. https://www.sciencedirect.com/science/article/pii/S0038092X2200072X

Léon JF, Barthélémy Akpo A, Bedou M, Djossou J, Bodjrenou M, Yoboué V, Liousse C (2021) PM2.5surface concentrations in southern West African urban areas based on sun photometer and satellite observations. Atmos Chem Phys 21(3):1815–1834. https://doi.org/10.5194/acp-21-1815-2021

Moomaw W, Yamba F, Kamimoto M, Maurice L, Nyboer J, Urama Kenya K, Fiji W, Bruckner T, Jäger-Waldau T, Pan A, J., van Ypersele J-P (2011) Renewable energy and climate change coordinating lead authors: lead authors: contributing authors: review editors

Mukkavilli SK, Prasad AA, Taylor RA, Troccoli A, Kay MJ (2018) Mesoscale Simulations of Australian Direct Normal Irradiance, Featuring an Extreme Dust Event. J Appl Meteorol Climatology 57(3):493–515. https://www.jstor.org/stable/26501002

Murphy AH (1988) Skill scores based on the mean square error and their relationships to the correlation coefficient. Mon Weather Rev 116:2417–2424

Niu GY, Yang ZL, Mitchell KE, Chen F, Ek MB, Barlage M, Kumar A, Manning K, Niyogi D, Rosero E, Tewari M, Xia Y (2011) The community Noah land surface model with multiparameterization options (Noah-MP): 1. Model description and evaluation with local-scale measurements. Journal of Geophysical Research. https://doi.org/10.1029/2010JD015139

Nooni IK, Tan G, Hongming Y, Saidou Chaibou AA, Habtemicheal BA, Gnitou GT (2022) Assessing the Performance of WRF Model in Simulating Heavy Precipitation Events over East Africa Using Satellite-Based Precipitation Product. Remote Sens 14(9) & Lim Kam Sian, K. T. C. https://doi.org/10.3390/rs14091964

Otkin JA, Greenwald TJ (2008) Comparison of WRF model-simulated and MODIS-derived cloud data. Mon Weather Rev 136(6):1957–1970. https://doi.org/10.1175/2007MWR2293.1

Overpeck JT, Meehl GA, Bony S, Easterling DR (2011) Climate data challenges in the 21st century. In *Science* (Vol. 331, Issue 6018, pp. 700–702). https://doi.org/10.1126/science.1197869

Patil R, Kumar P, P (2016) WRF model sensitivity for simulating intense western disturbances over Northwest India. Model Earth Syst Environ 2(2). https://doi.org/10.1007/s40808-016-0137-3

Peuch V-H, Engelen R, Rixen M, Dee D, Flemming J, Suttie M, Ades M, Agustí-Panareda A, Ananasso C, Andersson E, Armstrong D, Barré J, Bousserez N, Dominguez JJ, Garrigues S, Inness A, Jones L, Kipling Z, Letertre-Danczak J, Thépaut J-N (2022) The Copernicus Atmosphere Monitoring Service: from research to operations. Bull Am Meteorol Soc. https://doi.org/10.1175/bams-d-21-0314.1

Prasad AA, Kay M (2020) Assessment of simulated solar irradiance on days of high intermittency using WRF-solar. Energies 13(2). https://doi.org/10.3390/en13020385

Reid JS, Eck TF, Christopher SA, Hobbs P, Holben B (1999) Use of the Ångstrom exponent to estimate the variability of optical and physical properties of aging smoke particles in Brazil. J Geophys Res Atmos 104(D22):27473–27489. https://doi.org/10.1029/1999JD900833

Ruiz-Arias JA (2020) Bias in modeled solar radiation by non-resolved intra-daily AOD variability. Sol Energy 205:221–229. https://doi.org/10.1016/j.solener.2020.04.082

Sarr MA, Gachon P, Seidou O, Bryant CR, Ndione J, Comby J (2014) Inconsistent linear trends in Senegalese rainfall dataindices from 1950 to 2007. Hydrol Sci J. https://doi.org/10.1080/02626667.2014.916407

Sawadogo W, Bliefernicht J, Fersch B, Salack S, Guug S, Ogunjobi KO, Meilinger S, Kunstmann H (2023) Global Horizontal Irradiance in West Africa: Evaluation of the WRF-Solar Model in Convection-Permitting Mode with Ground Measurements. J Appl Meteorol Climatol 62(7):835–851. https://doi.org/10.1175/JAMC-D-22-0186.1

Sawadogo W, Fersch B, Bliefernicht J, Meilinger S, Rummler T, Salack S, Guug S, Kunstmann H (2024) Evaluation of the WRF-solar model for 72-hour ahead forecasts of global horizontal irradiance in West Africa: A case study for Ghana. Sol Energy 271. https://doi.org/10.1016/j.solener.2024.112413

Schuster GL, Dubovik O, Holben BN (2006) Ångstrom exponent and bimodal aerosol size distributions. J Geophys Res Atmos 111(7). https://doi.org/10.1029/2005JD006328

Senghor MW, Faye MN, Faye B, Diarra K, Elguero E, Gaye O, Bañuls AL, Niang AA (2011) Ecology of phlebotomine sand flies in the rural community of Mont Rolland (Thiès region, Senegal): Area of transmission of canine leishmaniasis. PLoS ONE 6(3). https://doi.org/10.1371/journal.pone.0014773

Shan Y, Shi H, Fan J, Lin L, Gao L, He C, Gao M, Miao L, Zhang L, Xia X, Chen H (2022) Revealing Bias of Cloud Radiative Effect in WRF Simulation: Bias Quantification and Source Attribution. J Geophys Research: Atmos 127(11). https://doi.org/10.1029/2021JD036319

Song G, Huva R, Xing Y, Zhong X (2021) WRF model moisture adjustment method: A case study with wintertime cloudy biases in Xinjiang, China. Weather Forecast 36(2):487–497. https://doi.org/10.1175/WAF-D-20-0117.1

Sosa-Tinoco I, Prósper MA, Miguez-Macho G (2022) Development of a solar energy forecasting system for two real solar plants based on WRF Solar with aerosol input and a solar plant model. Sol Energy 240:329–341. https://doi.org/10.1016/j.solener.2022.05.049

Tapakis RD, Charalambides AG (2013) Monitoring Cloud Motion in Cyprus for Solar Irradiance Prediction. Conf Papers Energy 2013:1–6. https://doi.org/10.1155/2013/320618

Thompson G, Eidhammer T (2014) A study of aerosol impacts on clouds and precipitation development in a large winter cyclone. J Atmos Sci 71:3636–3658. https://doi.org/10.1175/JAS-D-13-0305.1

Thompson G, Tewari M, Ikeda K, Tessendorf S, Weeks C, Otkin J, Kong F (2016) Explicitly Coupled Cloud Physics and Radiation Parameterizations and Subsequent Evaluation in WRF High-Resolution Convective Forecasts

Toure NO, Gueye NRD, Mbow-Diokhane A, Jenkins GS, Li M, Drame MS, Coker KAR, Thiam K (2019) Observed and Modeled Seasonal Air Quality and Respiratory Health in Senegal During 2015 and 2016. Geohealth 3(12):423–442. https://doi.org/10.1029/2019GH000214

United Nations Framework Convention on Climate Change (UNFCCC) (2020) Contribution déterminée au niveau national du Sénégal. https://unfccc.int/sites/default/files/NDC/2022-06/CDNSenegal*20approuv**Ae-pdf-.pdf__;JcOp!!NLFGqXoFfo8MMQ!oEaiyZNVslZJ12SMq3g7n5phTJy1U7er7WwFGjfSdPiBeU9X4N6st6ZyNZ1c1NBiOvZ3Ncrko1x_jT9N08IaHpkZIixHes$. Accessed 25 May 2025

Verbois H, Huva R, Rusydi A, Walsh W (2018) Solar irradiance forecasting in the tropics using numerical weather prediction and statistical learning. Solar Energy 162:265–277. https://doi.org/10.1016/j.solener.2018.01.007

Yang J, Kim J-H, Jiménez PA, Sengupta M, Dudhia J, Xie Y, Golnas A, Giering R (2021) An efficient method to identify uncertainties of WRF-Solar variables in forecasting solar irradiance using a tangent linear sensitivity analysis. (2021). https://www.elsevier.com/open-access/userlicense/1.0/

Youm I, Sarr J, Sall M, Kane MM (2000) Renewable energy activities in Senegal: a review. www.elsevier.com/locate/rser

Zhang M, Bretherton C (2008) Mechanisms of low cloud-climate feedback in idealized single-column simulations with the Community Atmospheric Model, version 3 (CAM3). J Climate 21(18):4859–4878. https://doi.org/10.1175/2008JCLI2237.1

Zhao C, Liu X, Leung LR, Hagos S (2011) Radiative impact of mineral dust on monsoon precipitation variability over West Africa. Atmos Chem Phys 11(5):1879–1893. https://doi.org/10.5194/acp-11-1879-2011